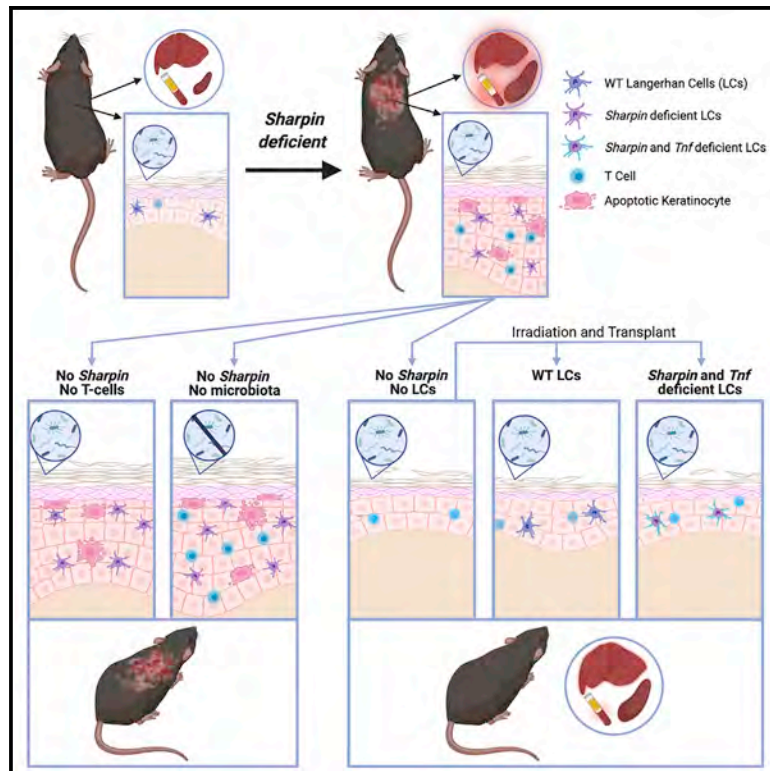


Langerhans cells are an essential cellular intermediary in chronic dermatitis

Graphical abstract



Authors

Holly Anderton, Michaël Chopin, Caleb A. Dawson, ..., Natasha Silke, Najoua Lalaloui, John Silke

Correspondence

silke@wehi.edu.au

In brief

TNF can be a potent cause of skin inflammation, but the origin of disease-causing TNF often remains elusive. Anderton et al. identify Langerhans cells (LCs) as the source of TNF responsible for dermatitis in *Sharpin^{cpdm}* mice, highlighting a T cell-independent, microbiota-independent role for LCs in driving TNF-mediated skin inflammation.

Highlights

- *In vivo* depletion of LCs in *Sharpin^{cpdm}* mice prevents TNF-mediated dermatitis
- The *Sharpin^{cpdm}* dermatitis phenotype is microbiota independent
- *Sharpin* mutation on LCs is necessary for the dermatitis-causing pathological effect
- *Sharpin* mutant LCs need to express TNF for the effect to occur



Article

Langerhans cells are an essential cellular intermediary in chronic dermatitis

Holly Anderton,^{1,2} Michaël Chopin,^{1,2} Caleb A. Dawson,^{1,2} Stephen L. Nutt,^{1,2} Lachlan Whitehead,^{1,2} Natasha Silke,^{1,2} Najoua Lalaloui,^{1,2,3} and John Silke^{1,2,3,*}

¹The Walter and Eliza Hall Institute for Medical Research, Parkville, Melbourne, VIC 3050, Australia

²Department of Medical Biology, University of Melbourne, Parkville, VIC 3050, Australia

³Senior author

*Correspondence: silke@wehi.edu.au

<https://doi.org/10.1016/j.celrep.2022.110922>

SUMMARY

SHARPIN regulates signaling from the tumor necrosis factor (TNF) superfamily and pattern-recognition receptors. An inactivating *Sharpin* mutation in mice causes TNF-mediated dermatitis. Blocking cell death prevents the phenotype, implicating TNFR1-induced cell death in causing the skin disease. However, the source of TNF that drives dermatitis is unknown. Immune cells are a potent source of TNF *in vivo* and feature prominently in the skin pathology; however, T cells, B cells, and eosinophils are dispensable for the skin phenotype. We use targeted *in vivo* cell ablation, immune profiling, and extensive imaging to identify immune populations driving dermatitis. We find that systemic depletion of Langerin⁺ cells significantly reduces disease severity. This is enhanced in mice that lack Langerhans cells (LCs) from soon after birth. Reconstitution of LC-depleted *Sharpin* mutant mice with TNF-deficient LCs prevents dermatitis, implicating LCs as a potential cellular source of pathogenic TNF and highlighting a T cell-independent role in driving skin inflammation.

INTRODUCTION

Innate immune signalling is vital for maintaining skin homeostasis. Its dysregulation predisposes individuals to skin diseases. The linear ubiquitin chain assembly complex (LUBAC) is a critical E3 ligase complex comprising three proteins, HOIL, HOIP and SHARPIN, that regulates signaling from the tumor necrosis factor (TNF) superfamily and pattern-recognition receptors (PRRs). A loss-of-function mutation termed chronic proliferative dermatitis mutation (*cpdm*) in the SHARPIN-encoding gene results in a dermatitis phenotype that shares clinical and histopathological features with chronic eczema and psoriasis (HogenEsch et al., 1993). These mice also develop systemic inflammatory symptoms, including hyperplastic bone marrow and extensive myelopoiesis, resulting in elevated white blood cells and splenomegaly with a disorganized splenic structure. There is general atrophy of lymphoid tissues, and *Sharpin*^{*cpdm*} mice have no Peyer's patches. There is also multi-organ inflammation, including neutrophil and macrophage infiltration of the periportal and -venous regions of the liver (HogenEsch et al., 1993).

SHARPIN deficiency reduces LUBAC activity, impairing the recruitment of downstream signaling components, delaying and reducing activation of nuclear factor κ B (NF- κ B)- and AP1-dependent genes from TNF, CD40 L, and Toll-like receptor (TLR) signaling pathways, sensitizing cells to TNF-induced death (Gerlach et al., 2011; Ikeda et al., 2011; Kumari et al., 2014; Rickard et al., 2014; Teh et al., 2016; Tokunaga et al., 2011; Zak et al., 2011).

LUBAC-deficient patients share many characteristics of *Sharpin*^{*cpdm*} mice (Boisson et al., 2012, 2015; Oda et al., 2019).

A patient with bi-allelic truncation mutations in HOIP developed skin manifestations and splenomegaly and responded well to anti-TNF treatment (Oda et al., 2019). As predicted from studies of *Sharpin*^{*cpdm*} mice, primary cells from the patient had reduced levels of the other LUBAC components SHARPIN and HOIL.

We, and others, have previously shown that loss of TNF or TNFR1 prevents the dermatitis phenotype in *Sharpin*^{*cpdm*} mice, suggesting that TNF-induced TNFR1 signaling is the primary driver of the pathology (Gerlach et al., 2011; Kumari et al., 2014; Rickard et al., 2014). Crosses of *Sharpin*^{*cpdm*} to *Ripk3*^{*-/-*}, *Mik1*^{*-/-*}, and *Caspase8*^{*+/-*} or keratinocyte-restricted Fas-associated death domain (FADD) knockout mice showed that blocking keratinocyte cell death prevents the inflammatory phenotype (Kumari et al., 2014; Rickard et al., 2014). These results suggest a role for TNF/TNFR1-induced keratinocyte cell death in driving dermatitis; however, the source of the pathogenic TNF ligand is unknown.

In the skin immune cells, neurons, fibroblasts, and keratinocytes can all produce the highly potent cytokine TNF (Aggarwal, 2003; Bashir et al., 2009; Tracey et al., 2008). Anti-TNF biologics have revolutionized the treatment of many inflammatory diseases (Lis et al., 2014). In the dermatological space, TNF inhibitors are used to treat psoriasis, where detectable differences in TNF have been seen in lesional versus non-lesional skin (Caldarola et al., 2009; Chiricozzi et al., 2018; Zaba et al., 2007). Despite this, a meta-analysis of systemic inflammatory markers in psoriasis found that TNF was a poor marker of disease severity because the increases were modest and varied a lot from study to study (Dowlatshahi et al., 2013). Reports suggest that TNF



inhibitors can also provide relief for patients with other inflammatory skin diseases, including hidradenitis suppurativa (HS), pityriasis rubra pilaris, and pyoderma gangrenosa (Greuter et al., 2017; Petrof et al., 2013; Speeckaert et al., 2019). Mildly elevated TNF has been reported in lesional lichen planus (Akpınar Kara, 2017) and detected in *ex vivo* skin culture media from biopsied HS lesions (Vossen et al., 2019; Zee et al., 2011). That said, circulating or lesional TNF levels are often not reported or are inconsistently elevated. Instead, the observed effect of treatment with TNF-targeting biologics is improved clinical symptoms and reduced expression of downstream cytokines such as interleukin-6 (IL-6), IL-17, IL-23, and IL-1 β . In summary, detecting differences in TNF levels in patients can be challenging. Even where TNF inhibitors provide relief the cellular source of pathological TNF remains elusive.

Immune infiltration is a prominent feature of the *cpdm* pathology, and immune cells can be a potent source of TNF *in vivo*. Transplanting *Sharpin^{cpdm}* bone marrow into wild-type (WT) mice does not induce dermatological disease, suggesting improper signaling due to SHARPIN deficiency in the haematopoietic compartment is insufficient for dermatitis (HogenEsch et al., 1993; Rickard et al., 2014). IL-5 depletion, which effectively reduces eosinophilia, did not ameliorate *cpdm* symptoms (Renninger et al., 2010), and crossing *Sharpin* mutant mice to T and B cell-deficient *Rag1^{-/-}* mice resulted in no reduction of the severity of the phenotype (Potter et al., 2014). These results imply that, despite their prominence, eosinophils, T cells, and B cells play no essential role in driving the disease.

Skin transplant experiments, transferring *Sharpin^{cpdm}* skin onto nude (Balb/c^{nu/nu}) or WT (C57BL/Ka) mice and WT or nude skin onto *Sharpin^{cpdm}* mice, showed that donor skin always retained the donor phenotype (Gijbels et al., 1995). Together, these results suggest that the defect resulting in dermatitis is skin intrinsic; however, they do not exclude a pathogenic contribution from the haematopoietic compartment. To address this question, we used the transgenic diphtheria toxin receptor (DTR) system. We crossed *Sharpin^{cpdm}* mice to CCR2-DTR (Hohl et al., 2009), CD11b-DTR (Cailhier et al., 2005), CD11c-DTR (Jung et al., 2002), or Langerin-DTR (Bennett et al., 2005) mice, enabling us to specifically deplete immune-cell subsets *in vivo* to determine their importance in the inflammatory phenotype. This revealed that Langerhans cells are crucial in promoting the cell-death-driven dermatitis phenotype in *Sharpin* mutant mice.

RESULTS

Characterization of the immune populations in the skin of *Sharpin^{cpdm}* mice

Despite the genetic experiments showing the dermatitis of *cpdm* mice is TNF dependent, there is no detectable difference in TNF in whole-skin lysates from *Sharpin^{cpdm}* mice versus control littermates at 11 weeks of age as measured by ELISA (Figure 1A). One explanation for this result is that only a small subset of cells in the skin produces pathogenic TNF. Infiltration by macrophages into the *Sharpin^{cpdm}* skin is an early event, coinciding with early keratinocyte cell death (Rickard et al., 2014) and the accumulation

of CD45⁺ immune cells in the dermis of *Sharpin^{cpdm}* mice by 3 weeks of age (Figure 1B).

We characterized the cellular infiltrate of the *Sharpin^{cpdm}* skin during early macroscopic disease to find enriched populations worth further investigation. To characterize T cell and myeloid compartments, we prepared whole skin for flow-cytometry analysis and stained cells for CD45, T cell receptor beta (TCR β), TCR $\gamma\delta$, major histocompatibility complex class II (MHCII), CD11b, CD11c, CD64, XCR1, EPCAM, and propidium iodide (PI) (Figures 1C and 1D). This revealed a 4-fold increase in live CD45⁺ cells (Figure 1C, first panel). There was a relative increase in $\alpha\beta$ T cells and a decrease in $\gamma\delta$ T cells as a percentage of CD45⁺ cells in whole skin, suggesting that $\alpha\beta$ T cells are preferentially activated in this context (Figures S1A and S1B). However, as crossing *Sharpin^{cpdm}* to the mature T and B cell-deficient *Rag1^{-/-}* mice results in no reduction of disease severity (Potter et al., 2014), this perturbation in $\alpha\beta$ T cells is likely to be a consequence of the phenotype, not a cause.

Consistent with our previously published histological observations (Rickard et al., 2014), there was an increase in the proportion of macrophages (CD45⁺CD64⁺CD11b⁺) in the skin of *Sharpin^{cpdm}* mice compared with controls (Figure 1E). There was also an increase in CD45⁺MHCII⁺CD11c⁺ dendritic cells (DCs), with the EPCAM⁺ Langerhans cell (LC) population (CD45⁺CD64⁻MHCII⁺CD11c⁺CD11b⁺XCR1⁻EPCAM⁺) being proportionally more highly elevated than cDC1 (CD45⁺CD64⁻MHCII⁺CD11c⁺XCR1⁺) or cDC2 (CD45⁺CD64⁻MHCII⁺CD11c⁺XCR1⁻) (Figure 1C). The increase in DCs was observed in both the dermis and the epidermis when digested and analysed separately (Figure 1E). The epidermal MHCII⁺CD11c⁺ cells in *Sharpin^{cpdm}* mice were larger and more “granular” than their WT counterparts, with a greater forward scatter (FSC) and side scatter (SSC), respectively (Figure 1F), potentially suggesting a different metabolic or proliferative state.

Chronic systemic depletion of CCR2-expressing cells in *Sharpin^{cpdm}* mice delays, but does not prevent, the onset of dermatological disease

To see if the enrichment in macrophages and DCs is a cause or a consequence of the disease, we used transgenic DTR-expressing mouse strains where cell-type-specific gene promoters drive the expression of a primate DTR. Mutations on murine DTR prevent receptor interaction making normal mouse cells 10³–10⁵ times more resistant to diphtheria toxin (DT) than primate cells. Injection of DT kills only cells expressing the high-affinity transgenic DTR (Bennett et al., 2005; Bennett and Clausen, 2007; Cailhier et al., 2005; Hohl et al., 2009; Jung et al., 2002).

We crossed the *Sharpin^{cpdm}* mice to CD11b-DTR (*Cd11b^{DTR}*) and CCR2-DTR (*Ccr2^{DTR}*) mice. CD11b (integrin alpha M [ITGAM]) is a surface marker expressed at high levels on macrophages. CCR2 is a chemokine receptor for the monocyte chemo-attractant protein (MCP) family, including MCP1, which was one of the chemokines significantly increased in skin lysates from *Sharpin^{cpdm}* mice (Rickard et al., 2014). It is also a marker of inflammatory monocytes and DCs typically recruited to inflamed tissues (Geissmann et al., 2003; Tsou et al., 2007, p. 2).

While *Sharpin^{cpdm}Cd11b^{DTR}* animals treated thrice weekly with DT had a mild delay in symptom onset, overall clinical scores

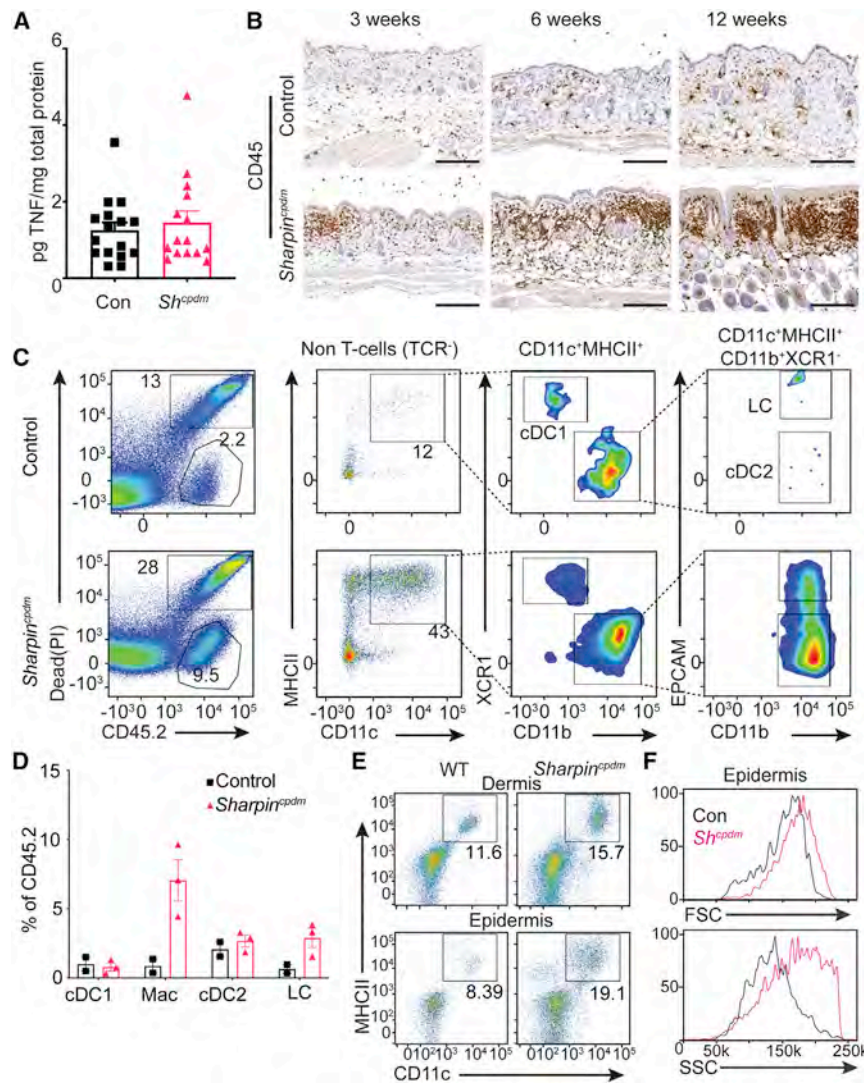


Figure 1. Immune-cell characterization in the skin of SHARPIN-deficient mice

(A) TNF in whole skin from *Sh^{cpdm}* (*Sh^{cpdm}*) versus control (Con) mice.

(B) Immunohistochemistry (IHC) analysis of dorsal skin from Con and *Sh^{cpdm}* mice over time. Scale bar, 200 μ m.

(C) Flow-cytometry gating strategies to identify LCs in 5-week-old mice.

(D) DC and macrophage quantification as a percentage of CD45.2 cells.

(E) Representative fluorescence-activated cell sorting (FACS) plots of the epidermis and dermis from 11-week-old mice. Gated population is MHCII⁺CD11c⁺ LCs.

(F) Representative histograms of forward scatter (FSC) and side scatter (SSC) of MHCII⁺CD11c⁺ cells from the indicated strains.

Graphs in (A) and (D) show mean \pm SEM, and each data point represents one mouse. See also Figure S1.

type, indicating that another cellular source is driving the inflammation.

Local depletion of DCs reduces skin phenotype in *Sharpin^{cpdm}* mice

As our flow-cytometry analysis of the *Sharpin^{cpdm}* mice suggested increased numbers of CD11c⁺ DCs (Figures 1D and 1E), we decided to investigate the overall contribution of DCs to the *Sharpin^{cpdm}* skin phenotype. We crossed CD11c-DTR (*Cd11c^{DTR}*) mice to the *Sharpin^{cpdm}* mice. *Cd11c^{DTR}* mice cannot tolerate multiple doses of DT administered systemically (Bennett and Clausen, 2007). The usual workaround for this is to generate bone marrow chimeric mice. However, *Sharpin^{cpdm}* mice develop microscopic phenotype as early as 3 weeks of age and macroscopic phenotype by 5 weeks,

(Table 1) tracked with *Sharpin^{cpdm}* (Figures 2A and 2B). This may be attributable to poor clearance of CD11b⁺ cells in the skin. Macrophages (F4/80) were detected in *Sharpin^{cpdm}**Cd11b^{DTR}* skin treated with DT for 8 weeks, despite efficient clearance of circulating cells (Figures 2C, 2D, and S2). While no conclusions can be drawn from these data about the importance of CD11b⁺ cells localized to the skin, our results show that circulating CD11b⁺ cells are not important in the *cpdm* phenotype.

In contrast, chronic depletion of CCR2-expressing cells caused a moderate reduction in onset that resulted in a significantly lower clinical score by endpoint (Figures 2A and 2B). We saw a reduction in T cell infiltration (CD3) into the epidermis and in epidermal proliferation (Ki67); however, most of the histological hallmarks of typical *Sharpin^{cpdm}* endpoint mice were present (Figures 2D and S2). Overall, these results suggest that ablation of monocytes, monocyte-derived macrophages, and monocyte-derived DCs had only a mild effect on the skin pheno-

which is before they would be old enough for transplant. We instead administered DT injections subcutaneously into the dorsal area from 3 to 11 weeks of age. Despite the presence of trauma-related phenotype at the puncture site (Koebner phenomenon; Figure 3A, small red circle), there was a distinct local reduction in lesion formation at the site of the injection bolus (Figure 3A, large green circle) and a measurable difference in phenotype severity at the endpoint (Figure 3B).

The local rescue was also seen histologically with reduced T cells (CD3), epidermal hyperplasia, and apoptotic (cleaved caspase-3 [CC3]) and proliferating (Ki67) keratinocytes in the injection area (Figures 3C and S3). Areas further from the site of the injection bolus had pathological signs of disease, such as epidermal hyperplasia (Figure 3C). However, the macroscopic rescue did extend beyond the injection site, most notably in the area under the chin, which is usually severely affected at endpoint (Figure 3A, inset).

Table 1. Clinical scoring of CPD in SHARPIN-deficient mice

Score	Description
0	no signs of dermatological disease, though there may be other signs of inflammatory disease, including uveitis and splenomegaly
1	mice have very early indications of disease; fur may be slightly scruffy looking, particularly in the dorsal region; no lesions, possibly some signs of flaky skin (like dandruff)
2	fur is scruffy, and there may be mild fur loss in the dorsal area; there is flaky skin when the fur is parted but no lesions; skin will feel thickened when the mouse is restrained
3	there is fur loss in the dorsal area and small but isolated lesion formation; the lesions are dry/not open; there may be micro, open lesions around the chin, but they scab over within a day; skin will feel thick and may be difficult to scruff due to adhesions of the skin to the underlying tissue; the mouse should not be scratching constantly but may occasionally; minimal redness
4	advancing lesions result in larger confluent areas of scabiness; there may be a few open lesions that quickly scab over; redness is more severe, as is scratching behaviour; dermatitis affecting the eyes or mouth may warrant ethical intervention at this point
5	severe, confluent lesions with multiple open lesions are continuously present; area around the mouth is typically very inflamed; severe redness even where there is not an open lesion; ethical endpoint

Systemic depletion of LCs rescues the skin but not the systemic phenotype of *Sharpin*^{cpdm}

One major group of immune cells resident in the epidermis are LCs. Given the rescue after local reduction of CD11c-expressing cells and considering the increased presence of LCs in both early and late disease (Figures 1C and 1D), we further examined their role in the *cpdm* mice. We crossed *Sharpin*^{cpdm} to langerin-DTR (*Lang*^{DTR}) mice and injected DT intraperitoneally twice weekly from 3 to 11 weeks old. All DT-treated *Sharpin*^{cpdm}*Lang*^{DTR} mice showed no overt signs of disease up to 60 days old, but after 5 weeks of DT treatment, 7 of 12 *Sharpin*^{cpdm}*Lang*^{DTR} mice developed mild phenotype. The other 5 showed no overt signs of disease by the typical endpoint (Figures 4A and 4B).

Langerin staining of epidermal ear sheets from DT-treated *Sharpin*^{cpdm}*Lang*^{DTR} mice with no overt signs of phenotype indicated that the LCs were wholly removed throughout DT treatment (Figures 4C and 4D). Epidermal ear sheet staining of *Cd11b*^{DTR} mice or the *Ccr2*^{DTR} mice showed an intact epidermal LC population after 3 doses of DT, 48 hours apart, suggesting that the LC population was not sensitive to DT in those models (Figures S4A and S4B). Flow-cytometry analysis of skin collected from DT-treated *Sharpin*^{cpdm}*Lang*^{DTR} mice that devel-

oped mild disease revealed some remaining LCs after 8 weeks of DT, though they were reduced compared with *Sharpin*^{cpdm} controls (Figure S4C). This suggests that the appearance of the symptoms in mice that developed mild skin lesions could be due to incomplete LC depletion during DT treatment.

Consistent with the macroscopic reduction of the skin phenotype, histopathology of LC-depleted *Sharpin*^{cpdm}*Lang*^{DTR} mice showed a reduction in epidermal hyperplasia, proliferating keratinocytes (Ki67), CC3⁺ keratinocytes, and CD45⁺ cells when compared with non-depleted *Sharpin*^{cpdm}*Lang*^{DTR} (Figures 4E and S4D).

As LC depletion, when started before onset of overt disease, prevented dermatitis symptoms, we examined a more clinically relevant setting by depleting LCs after mice developed dermatological disease. Remarkably, even when DT treatment was started after visible signs of skin disease, LC ablation resulted in a marked slowing of disease progression, though symptoms were not reversed by the treatment (Figures 4F and 4G).

More surprisingly, depletion of LCs also affected other inflammatory symptoms seen in *Sharpin*^{cpdm} mice. DT-treated *Sharpin*^{cpdm}*Lang*^{DTR} males had slightly increased body weight (Figure 4H), and while splenic architecture remained disturbed, spleen weights were reduced in LC-depleted mice (Figures 4I and 4J). Like the non-depleted *Sharpin*^{cpdm} mice, LC-depleted *Sharpin*^{cpdm} mice had elevated white blood cells compared with controls. However, the absolute white blood cell count was significantly less than in non-depleted *Sharpin*^{cpdm} mice, and lymphocytes and eosinophils were significantly reduced (Figure 4K). This reduction in circulating immune cells upon LC depletion suggests that increased bone marrow output is a consequence of the skin phenotype, not a cause.

Genetic depletion of LCs rescues the skin phenotype of the *Sharpin*^{cpdm} mice

DT-induced depletion of langerin-expressing cells is not limited to epidermal LCs, as there is a functionally distinct population of langerin-expressing dermal DCs (Kaplan, 2010; Nagao et al., 2009). Furthermore, DT treatment does not start until after weaning, by which stage the mice already show microscopic signs of disease (Rickard et al., 2014). We recently generated and characterized *Suz12*^{lox/lox}*Cre*^{Cd11c} (hereafter *Suz12*^{Cd11c}) mice (Zhan et al., 2021), which allowed us to circumvent these issues. These mice lack the Suz12 protein, a component of the polycomb repressor complex 2, in cells expressing CD11c (Zhan et al., 2021). The loss of Suz12 disrupts the ability of LCs to replicate and populate the epidermis, which leads to the sustained loss of the LC network in the skin soon after birth (Figure 5A). Notably, loss of Suz12 in CD11c-expressing cells does not affect the development or function of other types of DCs found in the skin, including the langerin-expressing dermal DC population (Zhan et al., 2021). By crossing *Sharpin*^{cpdm} mice to these *Suz12*^{Cd11c}ΔLC mice, we were able to assess the specific role of LCs before disease onset.

Mice without epidermal LCs had no macroscopic dermatitis at the typical *Sharpin*^{cpdm} endpoint of 11 weeks, though some mice eventually developed a mild phenotype (Figures 5B and 5C). The systemic inflammatory phenotype was again reduced. Bodyweights of both males and females were closer to WT than

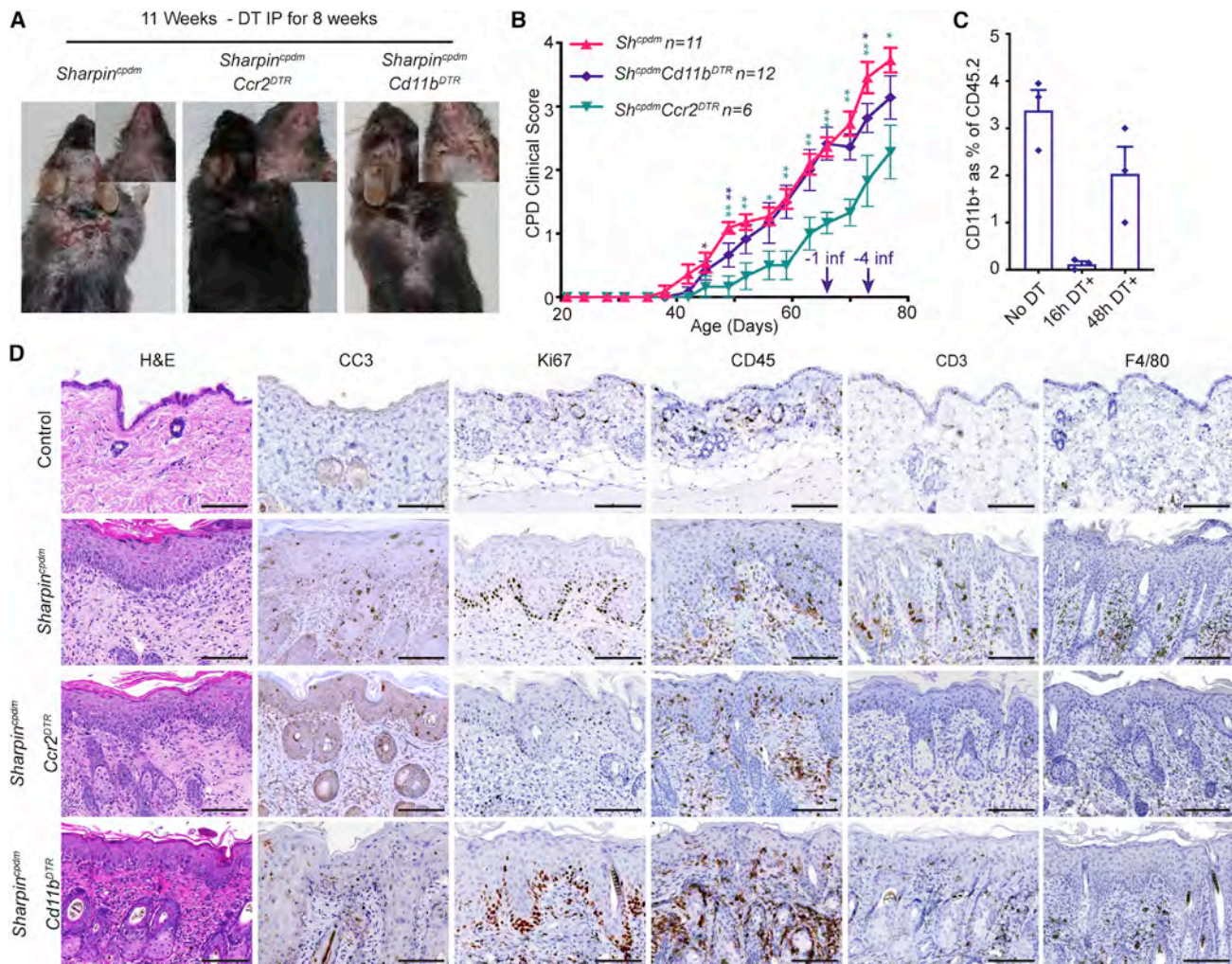


Figure 2. Phenotypic analysis of CCR2- or CD11b-depleted *Sharpin^{cpdm}* mice

(A) Representative images of mice of the indicated genotypes after 8 weeks of DT treatment. (B) Clinical scoring of dermatitis throughout DT treatment. Note: 1 mouse on D66 and 4 mice on D73 in the CD11b-depletion cohort were removed due to infection (inf). Asterisk (*) indicates that the line of matching color is significantly different from the *Sharpin^{cpdm}* line (pink) at the associated time point (Mann-Whitney U test). * $p \leq 0.05$, ** $p \leq 0.01$. (C) CD11b⁺ cells as a percentage of CD45.2⁺ in blood following acute depletion of CD11b population with DT. Each data point represents one mouse. (D) Representative H&E and IHC analyses of dorsal skin from the indicated genotypes at the experimental endpoint. Scale bars, 100 μ m. Graphs in (B) and (C) show mean \pm SEM. See also Figure S2.

Sharpin^{cpdm} controls (Figure 5D). Immune infiltrates in the liver still feature in the *Sharpin^{cpdm}Suz12^{Cd11c} Δ LC* mice; however, they were reduced compared with *Sharpin^{cpdm}Suz12^{wt}* littermates (Figure 5E). The splenic structure remained disorganized; however, the severity of splenomegaly was significantly less than *Sharpin^{cpdm}Suz12^{WT}* (Figures 5E and 5F). Blood analysis showed significant reductions in absolute white blood cell count and all subpopulations (Figure 5G). While it is possible that cDC1 depletion in the spleen and lymph nodes upon DT treatment contributed to the reduced systemic phenotype in the *Sharpin^{cpdm}Lang^{DTR}* cross, the *Sharpin^{cpdm}Suz12^{Cd11c} Δ LC*, with their intact cDC1 population, had a more profound improvement in the systemic phenotype. This strongly supports the conclusion that cDC1 depletion is not responsible for the systemic improvement.

Histologically, at 11 weeks of age, most skin samples showed none of the characteristic pathological features of the *Sharpin^{cpdm}* phenotype (Figures 5H and S5A). However, occasional small areas presented mild thickening of the epidermis accompanied by increased keratinocyte death and proliferation, accumulations of CD45⁺ cells in the associated papillary dermis, and T cell exocytosis into the epidermis (Figure 5H, mild pathology). The presence of mild histological disease at 11 weeks of age tracks with the eventual development of phenotype seen in some of the *Sharpin^{cpdm}Suz12^{Cd11c} Δ LC* from 90 days onward (Figures 5B and 5C). None of these mice developed typical endpoint phenotype; instead, the phenotype was present in patches, which, in some cases, developed into deep lesions, while adjacent areas remained symptom free even on histology (Figure 5I).

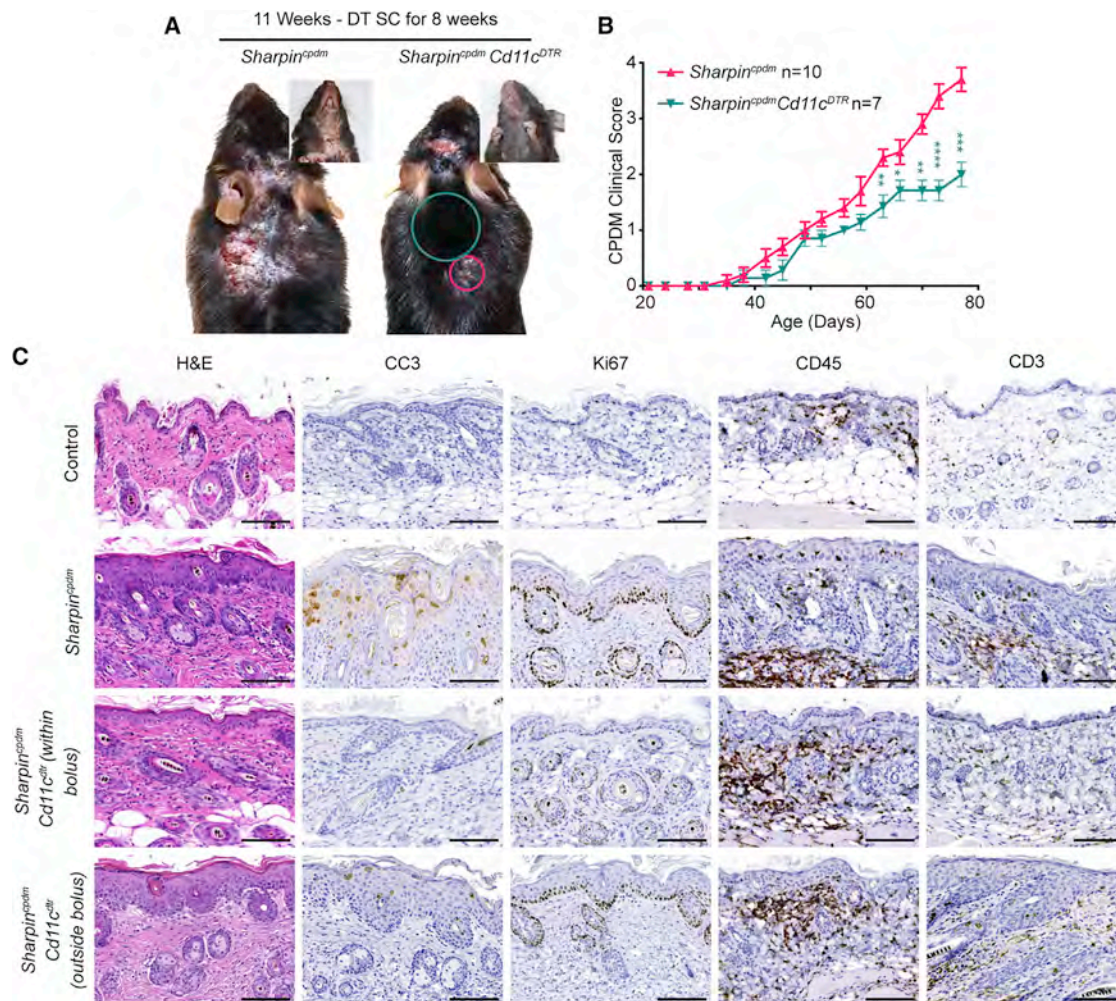


Figure 3. Phenotypic analysis of CD11c-depleted *Sharpin*^{cpdm} mice

(A) Representative images of mice of the indicated genotypes at the experimental endpoint.

(B) Clinical scoring of dermatitis during DT treatment. Data points are mean ± SEM. Significance by Mann-Whitney U ; *p ≤ 0.05, **p ≤ 0.01, ***p ≤ 0.001, ****p < 0.0001.

(C) H&E and IHC analyses of dorsal skin from the indicated genotypes at experimental endpoint. Scale bars, 100 μm. See also Figure S3.

Intriguingly, epidermal ear sheets from older (aged 23+ weeks) *Sharpin*^{cpdm}*Suz12*^{Cd11c}ΔLC mice had small patches of LCs (Figure 5J) that appear to be clones of resident LCs that managed to proliferate to some extent. Therefore, it is notable that langerin⁺ cells were also present in areas of dorsal skin pathology as typified by epidermal hyperplasia and the presence of dying keratinocytes (Figure 5K), suggesting that the occasional late development of dermatitis symptoms in *Sharpin*^{cpdm}*Suz12*^{Cd11c}ΔLC mice is attributable to the presence of LCs.

***Sharpin*^{cpdm} mice develop dermatitis symptoms under germ-free conditions**

These results strongly suggest that LCs contribute to the *cpdm* pathology. Because LCs play a critical role in responding to the skin microbiome and SHARPIN regulates signals downstream of TLR signaling (Wang et al., 2012; Zak et al., 2011), we considered that TLR dysfunction in LCs could result

in a loss of commensal tolerance. However, when *Sharpin*^{cpdm} mice were raised in germ-free isolators, they developed dermatological symptoms on a similar timeline and with equal severity compared with those in specified-pathogen-free (SPF) colonies (Figure 5L). This shows that the response to the microbiome does not play a significant role in the *Sharpin*^{cpdm} phenotype.

Nerve attrition is not responsible for reducing dermatitis when LCs are ablated

There is evidence that nerve cells play a role in inflammatory signalling in the skin. Neurons can participate in innate immune responses, and there appears to be some functional crossover between neurons and innate immune cells (Cohen et al., 2020). Innervation is required for a psoriasis-like response in the KC-Tie2 psoriasisform mouse model (Ostrowski et al., 2011), and there is a reported morphological association between nerve

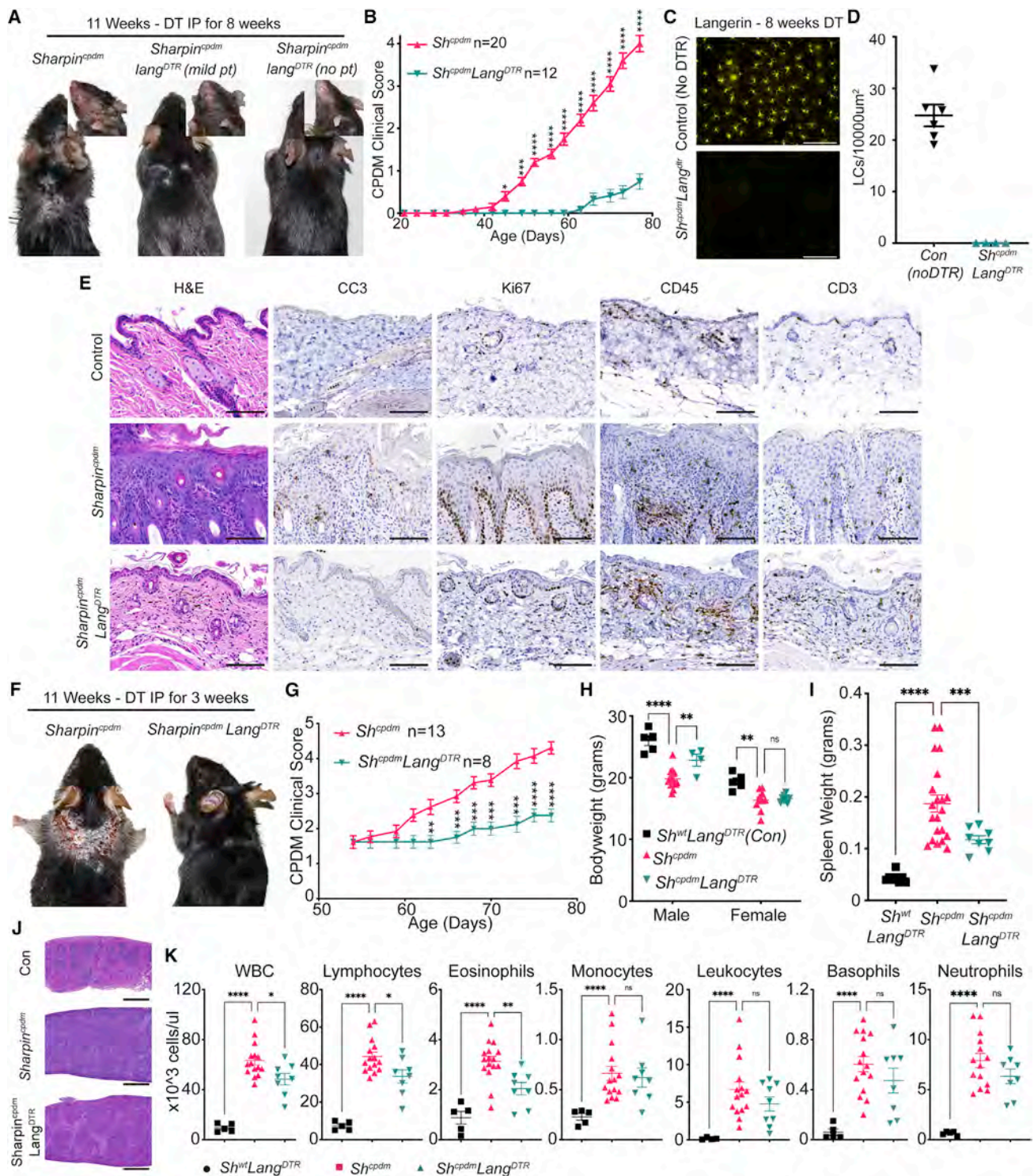


Figure 4. Phenotypic analysis of langerin-depleted *Sharpin^{cpdm}* mice

(A) Representative images of mice of the indicated genotypes at experimental endpoint.

(B) Clinical scoring of dermatitis during DT treatment. Data points are mean ± SEM (Mann-Whitney U test).

(C) Representative langerin immunofluorescence (IF) staining of epidermal ear sheets from *Sh^{cpdm}Lang^{DTR}* and DTR-negative control mice after 8 weeks of DT. Scale bars, 50 μm.

(D) Quantification of LCs in ear sheets from chronic DT-treated mice. Each data point represents one mouse; average LC count from 12–20 100 × 100 μm fields.

(legend continued on next page)

fibers and LCs in psoriasis vulgaris and lichen simplex chronicus (Cui et al., 2009). DT-induced depletion of LCs reduced the number of sensory axons in the mouse footpad (Doss and Smith, 2014). Thus, it was possible that loss of skin innervation was causal or contributed to the dramatic reduction in inflammation caused by the depletion of LCs in *Sharpin^{cpdm}* mice. To test this, we stained the *Sharpin^{cpdm}Suz12^{Cd11c}* ΔLC and LC-depleted *Sharpin^{cpdm}Lang^{DTR}* mice for the neuronal marker PGP9.5. Consistent with previous reports (Doss and Smith, 2014), epidermal nerves were reduced upon DT-induced LC depletion. However, the *Sharpin^{cpdm}Suz12^{Cd11c}* ΔLC mice, despite the absence of LCs, were innervated throughout the epidermis (Figure S5B) even without LCs, indicating that the reduction in phenotype due to LC depletion was not due to epidermal nerve attrition (Figure S5C).

Imaging of *Sharpin^{cpdm}* whole-skin mounts shows LC accumulations in the epidermis

To study the localization, behavior, and motility of LCs, we performed live *in vivo* imaging of the ears of endpoint *Sharpin^{cpdm}* mice and controls. This showed an increased density of MHCII⁺ cells in the epidermis (Figure 6A). Consistent with our earlier flow-cytometry analysis, *Sharpin^{cpdm}* LCs appeared larger and with more dendrites when compared with control mice (Figure 6B). However, they were not notably more motile than LCs in the ears of the control animals (Figures 6C and 6D).

While ears are ideal for live microscopy, they exhibit few disease symptoms (HogenEsch et al., 1993). To study LCs *in situ* throughout the initiation and progression of the disease at a site of pathology, we performed three-dimensional (3D) imaging of intact dorsal skin at 3 different ages during the lifespan of the mice. Consistent with earlier studies (Ikeda et al., 2011; Rickard et al., 2014), as the disease progressed, we observed an increased frequency of keratinocyte cell death (Figures 6E and 6F). Furthermore, we observed patchy accumulations of MHCII⁺ cells with dendritic morphology in the mid and upper epidermis (Figures 6E, 6G, and 6H), coinciding with loss of epidermal tight junctions (Figures 6E, 6I, and 6J) and appearing frequently, though not exclusively, around hair follicles. Flow-cytometry analysis showed that while there is a population of MHCII⁺CD11c⁺Lang⁻ cells in the *Sharpin^{cpdm}* epidermis that is absent in the WT, they account for only 20% of MHCII⁺ cells observed (Figures 6K and 6L). This population is primarily GrLy6c⁻ and is thus unlikely to be inflammatory monocytes (Figures S6A and S6B). LCs make up the greatest proportion of MHCII⁺ cells, and a far greater proportion of them are proliferating in the *Sharpin^{cpdm}* mice than in the WT mice (Figures 6K and 6M). Together, these data suggest that the increase in LC density is primarily due to local proliferation. The mean fluores-

cent index of MHCII, CD80, and CD86 are increased in *Sharpin^{cpdm}* LCs, suggesting an activated population (Figure 6N). CD11c is also increased on *Sharpin^{cpdm}* LCs, while CD11b is notably reduced (Figure 6N).

Transplantation of WT bone marrow into langerin-depleted *Sharpin^{cpdm}* mice does not induce dermatitis

Taken together, our results support earlier work from skin transplant experiments indicating that the *Sharpin^{cpdm}* disease mechanism is skin intrinsic (Gijbels et al., 1995). However, because LCs are transplanted together with donor skin and renew themselves *in situ* (Gomez Perdiguerro et al., 2015; Merad et al., 2002), these experiments do not address whether LCs respond to the defective environment in the *Sharpin*-deficient skin or whether an intrinsic defect in *Sharpin*-deficient LCs drives disease. Bone marrow transplant experiments involving *Sharpin^{cpdm}* donors into WT animals also suffer from a similar drawback because LCs are resistant to irradiations used to ablate the recipient's hematopoietic system and therefore are not replaced by the donor cells. Consequently, the importance of the *Sharpin* defect in LCs to driving disease is undefined.

Monocyte progenitors can enter the skin and differentiate into LCs when the LC niche is empty (Chopin and Nutt, 2015; Ginhoux and Merad, 2010). In order to determine if the *Sharpin* mutation in LCs is required to drive skin disease, we transplanted bone marrow from *Sharpin^{cpdm}* or UBC-GFP (functionally WT but ubiquitously expressing GFP) (Schaefer et al., 2001) mice into *Lang^{DTR}* mice treated with DT to render them LC deficient. As DT treatment is maintained after transplantation, monocyte-derived LCs from a non-DTR expressing donor (e.g., *Sharpin^{cpdm}*) can repopulate the epidermis while those from a DTR-expressing donor (e.g., *Sharpin^{cpdm}Lang^{DTR}*) cannot (Figure 7A). As expected, *Sharpin^{cpdm}Lang^{DTR}* mice transplanted with *Sharpin^{cpdm}* bone marrow recapitulated the typical *cpdm* phenotype, developing the same dermatological disease as non-transplanted mice (Figures 7B and 7C), therefore serving as a positive control. Critically, this was accompanied by a substantial repopulation of the LC niche in the dorsal area, a prominent region for the *cpdm* pathology (Figures 7D and S4A). On the other hand, transplantation of *Sharpin^{cpdm}* bone marrow into LC-depleted *Sharpin^{WT}Lang^{DTR}* mice developed no signs of phenotype clinically or histologically, indicating that the *Sharpin* mutation of LCs is insufficient for disease. DT-treated *Sharpin^{cpdm}Lang^{DTR}* mice transplanted with WT bone marrow also developed little (n = 1) to no (n = 2) visible signs of disease, suggesting that WT LCs in *Sharpin^{cpdm}* skin are insufficient to provoke dermatitis. Using UBC-GFP mice as the WT donors, we could confirm that the LCs present were of donor haematopoietic origin (Figure 7E). Consistent with our previous results,

(E) H&E and IHC analyses of dorsal skin from the indicated genotypes at experimental endpoint. Scale bar, 100 μm.

(F) Representative images of mice from the late-start experiment after 3 weeks of systemic DT.

(G) Clinical scoring dermatitis during DT treatment in the late-start experiment (Mann-Whitney U test).

(H–K) Systemic phenotype in langerin-depleted *Sh^{cpdm}* versus con mice at the experimental endpoint. Each data point represents one mouse. (H) Bodyweight,

(I) spleen weights, and (J) H&E of spleen. Scale bar, 1000 μm.

(K) Circulating white blood cell numbers. All mice, including the WT expressing DTR and *Sh^{cpdm}* without DTR, were treated with DT. All graphs show mean ± SEM; significance by one-way ANOVA; except where indicated.

See also Figure S4.

Sharpin^{cpdm}Lang^{DTR} bone marrow (BM) into *Sharpin^{cpdm}Lang^{DTR}* mice treated throughout with DT (Δ LC) developed mild disease, much milder than the positive control group but more severe than the mice transplanted with WT BM (Figures 7B and 7C). In these mice, the disease, while mild, was notably more severe than the same strain receiving DT treatment but without the transplant step (Figures 4A and 4B). The development of mild disease was not due to poor LC depletion (Figures 7D and S7A) and was likely the result of irradiation-induced TNF production by various skin cells, including keratinocytes (Müller and Meineke, 2007).

Reconstitution of WT T_{regs} in the WT transplant does not fully account for the absence of phenotype

Selective reintroduction of functional SHARPIN into *Sharpin^{cpdm}* regulatory T cells (T_{regs}) delays onset of the skin disease until after 3 months of age (Sasaki et al., 2019), which could account for the reduced phenotype in our WT BM transplant. Therefore, we transplanted with *Rag1^{-/-}* BM, which cannot reconstitute WT T_{regs}. These mice also developed mild clinical disease similar to those transplanted with *Sharpin^{cpdm}Lang^{DTR}* BM (Figures 7B and 7C).

Histological observations were consistent with the observations of macroscopic disease. DT-treated *Sharpin^{cpdm}Lang^{DTR}* mice transplanted with *Sharpin^{cpdm}* BM had significant epidermal hyperplasia, immune cell infiltrate, and keratinocyte apoptosis (Figures 7F and S7B). In contrast, the WT, *Sharpin^{cpdm}Lang^{DTR}* (Δ LC), and *Rag1^{-/-}* donor transplant groups had a reduction in all hallmarks (Figure 7F). The *Sharpin^{cpdm}Lang^{DTR}*(Δ LC) and *Rag1^{-/-}* donor transplanted mice all had some histological disease with mild to moderate epidermal hyperplasia and immune-cell infiltration. *Sharpin^{cpdm}Lang^{DTR}*(Δ LC) donor transplanted mice had scattered epidermal CC3 with occasional patches of high-frequency keratinocyte apoptosis. *Rag1^{-/-}* transplanted mice also had scattered CC3 but notably fewer high-intensity patches.

For unknown reasons, *Rag1^{-/-}* transplanted mice had fewer repopulated LCs at the time of collection than other reconstitutions (Figures 7D and S7A), although they were confirmed to be of donor origin (Figure 7E). However, sites of LC repopulation did not correspond with sites of increased histological severity. Co-staining for langerin and CC3 showed only occasional scattered keratinocyte apoptosis in areas with LCs, while patches with increased CC3 were more likely to be absent LCs (Fig-

ure S7C). This supports the idea that irradiation-induced inflammation leads to the mild phenotype seen in the transplanted mice and that, unlike in the *Sharpin^{cpdm}* transplanted mice, the presence of *Sharpin^{wt}* LCs did not worsen the inflammation. Indeed, the overall reduction in CC3 in the *Rag1^{-/-}* transplants compared with the *Sharpin^{cpdm}Lang^{DTR}* could indicate that even a partial replacement of *Sharpin^{cpdm}* LCs with *Sharpin^{wt}* LCs was able to moderate the post-irradiation inflammation even in the absence of WT T_{regs}.

Transplantation of *Sharpin^{cpdm}Tnf^{-/-}* into langerin-depleted *Sharpin^{cpdm}* mice also prevents dermatitis

While transplantation of *Sharpin^{cpdm}* BM into *Sharpin^{cpdm}Lang^{DTR}* mice recapitulated the *cpdm* phenotype, transplantation with *Sharpin^{cpdm}Tnf^{-/-}* BM prevented dermatitis to a similar degree as the WT and *Rag1^{-/-}* transplants (Figures 7B and 7C). In this experiment, transplanted LCs have the *Sharpin* mutation; however, they cannot produce TNF. On the other hand, local SHARPIN-deficient cells, including dermal fibroblasts and keratinocytes, remain capable of producing TNF. Histological markers of disease are almost absent (Figure 7F) and certainly far less evident than in the *Sharpin^{cpdm}Lang^{DTR}* (Δ LC) donor experiment. This suggests that even *Sharpin* mutant LCs can mitigate inflammation in the *Sharpin* mutant skin provided they cannot produce TNF. These results strongly support the idea that *Sharpin* mutant LCs are the cellular source of pathogenic TNF that typically drives the dermatitis phenotype.

DISCUSSION

We, and others, have previously established a key role for TNF-mediated cell death in promoting the *Sharpin^{cpdm}* lethal inflammatory phenotype. Previous studies show that the phenotype occurs in the absence of mature B and T cells (Potter et al., 2014), suggesting that an innate immune response drives skin inflammation. Our study reveals an unanticipated role for LCs in this innate inflammatory response. This is a striking discovery on several levels: firstly, because LCs are primarily thought to help maintain homeostasis or promote inflammation by regulating immune responses via activation and suppression of T cell populations (Eidsmo and Martini, 2018; Seneschal et al., 2012; van der Aar et al., 2013; West and Bennett, 2017). It is also remarkable that even though *Sharpin^{cpdm}* mice have many other cell types capable of producing TNF to induce keratinocyte

Figure 5. Phenotypic analysis of *Sharpin^{cpdm}Suz12^{cd11c}* mice

- (A) Langerin IF staining of epidermal ear sheets from mice of the indicated genotypes 48 h after DT. Scale bars, 100 μ m.
 (B) Representative images of mice of the indicated genotypes and ages.
 (C) Clinical scoring of dermatitis from weaning to endpoint. Mice removed from the scoring as indicated.
 (D–G) Systemic phenotype analysis at 11 weeks. Each data points represents one mouse. (D) Bodyweight. (E) Representative H&E of liver and spleen. Liver scale bar, 400 μ m; insert scale bar, 100 μ m; spleen scale bar, 1,000 μ m. (F) Spleen weight, and (G) numbers of circulating white blood cells as indicated.
 (H) H&E and IHC analysis of dorsal skin from the indicated genotypes at 11 weeks. Scale bars, 100 μ m.
 (I) H&E staining of *Sh^{cpdm}Suz12^{cd11c}* at 23 weeks showing an area with a lesion and immediately adjacent symptom-free area. Scale bar, 400 μ m.
 (J and K) IF staining of (J) langerin in epidermal ear sheet showing a patch and (K) langerin and CC3 in histologically affected dorsal skin of *Sharpin^{cpdm}Suz12^{cd11c}* at 23 weeks. Scale bars, 50 μ m. Dotted lines indicate the epidermis and dermis separation.
 (L) Germ-free *Sh^{cpdm}* mice develop dermatitis on a similar time frame to *Sh^{cpdm}* mice with normal microbiota (specified-pathogen-free [SPF]). Clinical scoring of the phenotype from weaning until endpoint; 1 germ-free *Sh^{cpdm}* mouse was removed on day 70 due to severe phenotype as indicated. All graphs show mean \pm SEM; significance by one-way ANOVA.
 See also Figure S5.

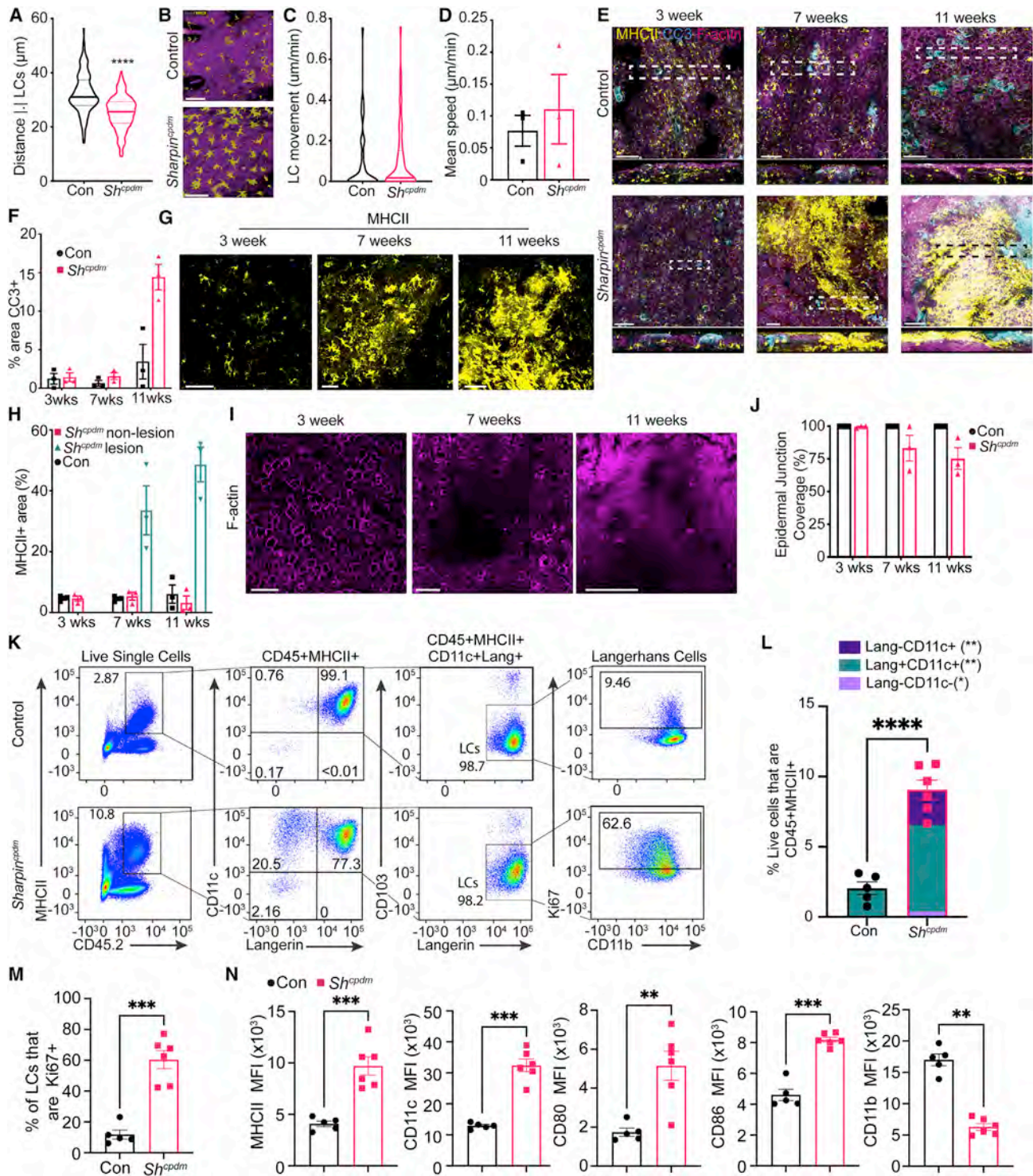


Figure 6. Live in vivo 2-photon and 3D ex vivo confocal microscopy of *Sharpin^{cpdm}* skin

(A and B) LC density and dendrites are increased in *Sharpin^{cpdm}* mice.

(A) Violin plot quantifying LC density in the ears during intravital imaging of 11-week-old mice of the indicated genotypes.

(B) Stills from intravital imaging showing ear collagen second harmonic generation (magenta) and LCs MHCII (yellow). Scale bar, 50 μ m.

(C) Quantification of LC motility during live imaging.

(D) Average LC movement speed during live imaging; each data point represents one mouse.

(legend continued on next page)

cell death, absence of LCs has as profound an effect as the ubiquitous loss of TNF and cell-death pathways, suggesting that the pathological TNF is LC derived. Thus, we have observed a direct, T cell-independent, microbiota-independent, pathogenic role for LCs in driving TNF-mediated skin inflammation.

The langerin DTR and Suz12 genetic-depletion experiments conclusively show that LCs drive dermatitis in SHARPIN-deficient mice: the most striking result is the tight correlation between the emergence of escapee LCs and the eventual onset of local patches of disease in both models. While previous work has shown that nerves in the skin can, when stimulated, cause inflammation (Cohen et al., 2020; Ostrowski et al., 2011) and that skin innervation is lost in *Lang^{DTR}* mice following DT treatment (Doss and Smith, 2014), our results clearly show that LC presence and skin innervation are separable, supporting the idea that LCs play a direct role in propagating inflammation. Whether acute LC loss affects innervation or nerve loss is linked to DT-induced LC cell death is unclear and would be interesting to explore further.

We, and others, have explored the contribution of various signaling and cell-death pathways to *Sharpin^{cpdm}* disease using ubiquitous and conditional knockout (KO) mouse strains (Gerlach et al., 2011; Berger et al., 2014; Rickard et al., 2014; Kumari et al., 2014; Anderton et al., 2017). The dermatological rescue seen in the *Sharpin^{cpdm}Suz12^{Cd11c}* mice (Figure 5) resembles the rescue we observed in *Sharpin^{cpdm}* mice with TNF or TNFR1 deficiency (Gerlach et al., 2011; Rickard et al., 2014). Interestingly, the similarity with *Tnfr1^{-/-}* extends to the unexpected reduction in systemic inflammation in *Sharpin^{cpdm}Suz12^{Cd11c}* mice (Rickard et al., 2014). This overlap strongly suggests that LCs in the skin are the critical source of TNF that induces keratinocyte cell death, which in turn worsens systemic inflammation. This supposition is further supported by the prevention of disease when *Sharpin^{cpdm}* mice are transplanted with *Sharpin^{cpdm}Tnf^{-/-}* BM.

As the skin is an essential barrier to pathogens, it is conceivable that affecting this barrier results in heightened systemic inflammation. Indeed, keratinocyte-specific loss of Notch, a key regulator of epidermal integrity, also induces dermatitis and systemic inflammation with many characteristics, such as splenomegaly and periportal liver inflammation, of SHARPIN-deficient mice (Demehri et al., 2008). However, the fact that *Sharpin^{cpdm}* mice in germ-free conditions suffer similar disease severity to *Sharpin^{cpdm}* mice in SPF conditions speaks against

the idea that systemic inflammation results from a disruption of the pathogen-excluding barrier function of skin in these mice. While our work shows that inflammation in the skin can be communicated to other organs in the absence of the microbiome and might be relevant when considering inflammatory comorbidities such as inflammatory bowel disease (IBD) and psoriasis, the mechanism remains unclear.

The precise role of LCs in mouse models of skin inflammation and in human disease remains controversial. These cells are the sentinels of the epidermis and are traditionally considered to be the first immunological line of defence against invading pathogens (Merad et al., 2008). Over the last decade, studies have suggested that immunoregulation, rather than immunostimulation, is a key function of LCs. Several groups suggest they have an anti-inflammatory effect, particularly during late-phase psoriasis-like disease (Kitashima et al., 2018; Terhorst et al., 2015), while others suggest that LCs contribute to inflammation in psoriasis-like disease by the production of IL-23 and promotion of Th17 phenotypes (Martini et al., 2017; Singh et al., 2016; Sweeney et al., 2016; Xiao et al., 2017). Seneschal et al. showed in human skin that LCs could promote tolerance by inducing activation and proliferation of T_{regs} but in the presence of foreign antigen will switch to promoting the activation and proliferation of effector memory T cells (Seneschal et al., 2012). Much of the current literature on LCs in inflammatory disease focuses on their roles in regulating immune responses via activation and suppression of T cell populations. However, *cpdm* is not dependent on T cells, and if LCs were instructing T_{regs}, then their absence should result in more disease, not less.

While the *Sharpin^{cpdm}* skin phenotype occurs in the absence of T cells, it is worth noting that selective reintroduction of functional SHARPIN into *Sharpin^{cpdm}* T_{regs} delays onset of the skin disease until after 3 months of age (Sasaki et al., 2019). Systemic Foxp3⁺ T_{regs} are reduced in *Sharpin^{cpdm}* mice (Teh et al., 2016), and chimeric BM transplant experiments suggest this is due to a cell-intrinsic defect in the *Sharpin^{cpdm}* T_{regs} resulting in defective thymic development (Park et al., 2016; Redecke et al., 2016). This suggests that T_{regs}' suppressive functions can potentially modulate, though not prevent, the innate-immune-driven dermatitis of the *Sharpin^{cpdm}* mice when they are present. However, in our models, T_{regs} are of the typical *Sharpin^{cpdm}* phenotype, i.e., reduced presence due to the intrinsic defect. Although LC depletion coincides with reduced numbers of CD3⁺ cells in *Sharpin^{cpdm}* skin and a reduction in inflammation, the reduction

(E) 3D *ex vivo* imaging of whole-skin mounts from mice of the indicated genotypes and ages. Top-down view is clipped to show epidermis only. Dotted boxes are viewed in cross-section below. Magenta is f-actin, yellow is MHCII, and blue is CC3. Scale bars, 100 μ m.

(F) Percentage of imaged epidermal area comprised of CC3⁺ cells measured directly from 2D snapshots.

(G) Magnified images of the epidermis from the MHCII-only channel of the *Sh^{cpdm}* mice over the time course. Scale bars, 50 μ m.

(H) Percentage of epidermal area comprised of MHCII⁺ cells, with lesional and non-lesional areas in *Sh^{cpdm}* mice distinguished by the loss of epidermal tight junctions in the former.

(I) F-actin-only channel of the *Sh^{cpdm}* mice over the time course. Scale bars, 100 μ m.

(J) Percentage of imaged epidermal area covered by epidermal tight junctions.

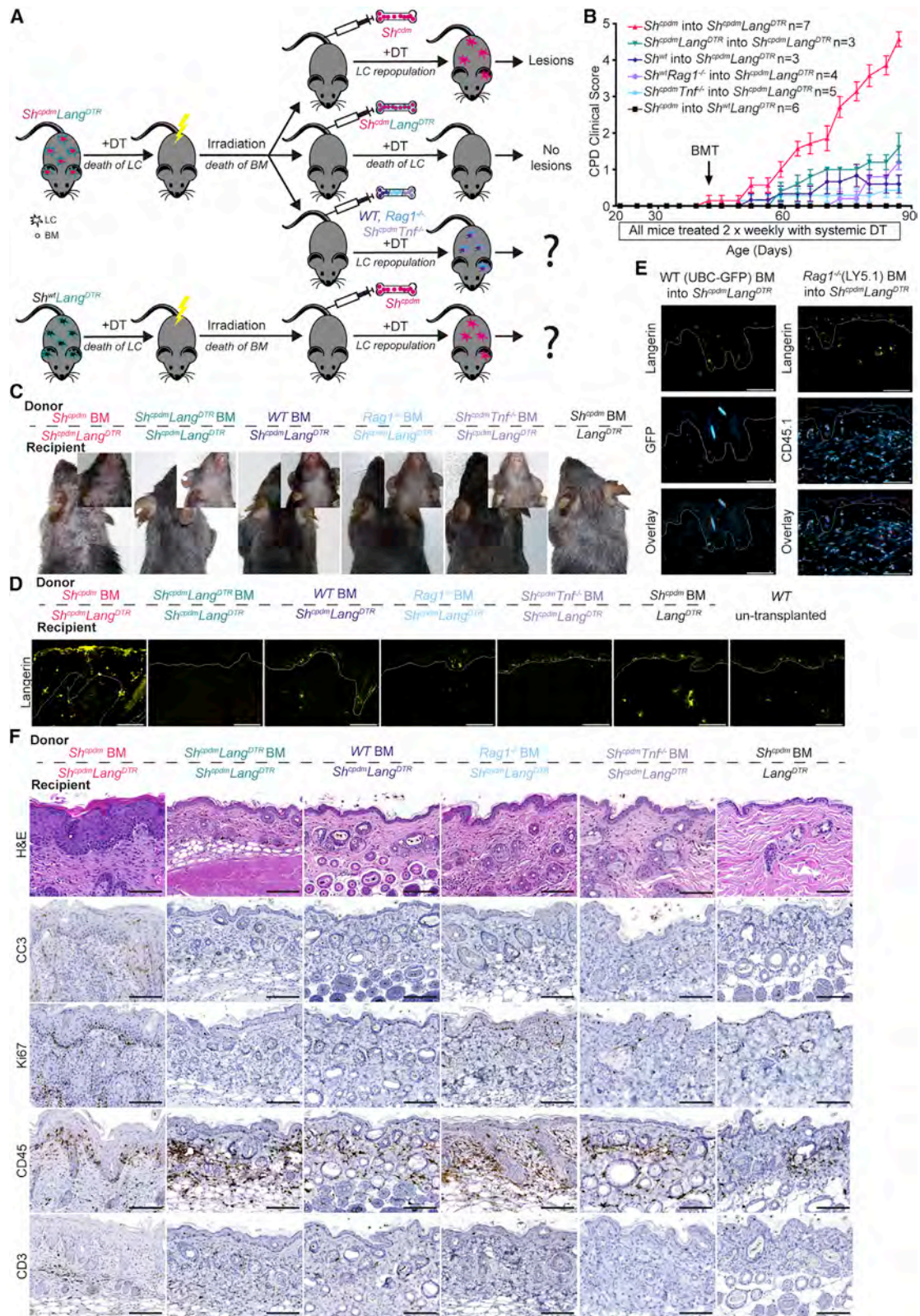
(K) Representative flow-cytometry and gating strategies to identify LCs in epidermis from the indicated genotypes at 11 weeks old.

(L) Percentage of live cells in the epidermis that are MHCII⁺, broken down based on the CD11c versus langerin sort in (K).

(M) Percentage of proliferating LCs in con versus *Sh^{cpdm}* in the epidermis at 11 weeks.

(N) Quantification of mean fluorescent index (MFI) for cell-surface markers as indicated. Graphs in (D), (F), (H), (J), (L), (M), and (N) show mean \pm SEM; each data point represents one mouse; significance by unpaired Welch's t test.

See also Figure S6.



(legend on next page)

in CD3⁺ is a consequence of the reduced inflammation rather than its cause. Transplantation of WT T_{regs} along with WT LCs from the UBC-GFP BM may account for the reduced phenotype in that transplant model; however, we also saw a reduction in disease severity when LC-depleted *Sharpin*^{cpdm} mice were transplanted with BM from *Rag1*^{-/-}, which were not able to fill the impaired T_{reg} niche. This supports the idea that the *Sharpin* defect on LCs is essential for their aberrant behavior.

Infiltrating and activated T cells are a feature of many inflammatory skin diseases (ISDs) and are often targeted with great success; however, T cell modulation therapies have also been associated with paradoxical induction of these same ISDs (Dogra et al., 2019; Komori et al., 2017; Maglie et al., 2018; Mössner and Pinter, 2020; Navarro-Triviño et al., 2020; Noell et al., 2017; Thompson et al., 2016). Cutaneous manifestations are also common in HIV/AIDs (Altman et al., 2015; Cedeno-Laurent et al., 2011), and psoriasis, typically considered to be a T cell-mediated disease, is associated with a paradoxical worsening of symptoms when T cell numbers drop as the disease gets more severe (Alpalhão et al., 2019; Cedeno-Laurent et al., 2011; Namazi, 2004). Pruritic papular eruption (PPE) is a pervasive skin manifestation of unknown aetiology in HIV/AIDs. Histologic findings include lymphocytic infiltrate, eosinophilia, mild epidermal hyperplasia, and spongiosis (Ekpe, 2019). PPE is considered a marker of advanced disease in adults as it typically worsens with low CD4 T cell counts. The manifestation and increasing severity of these conditions with decreasing T cell counts suggest that the pathology in these patients is not T cell driven, like the dermatitis associated with SHARPIN deficiency.

One interesting consideration is that LCs can serve as a reservoir of HIV (Matsuzawa et al., 2017; Mayr et al., 2017). It is possible that the viral status could affect LC inflammatory functions, potentially contributing to the cutaneous disease aetiology in that context. Patients with HIV-associated psoriasis often experience a reduction in psoriatic symptoms with a restoration of the T cell population by anti-retroviral treatment (Morar et al., 2010). However, our findings suggest that T cell recovery may be only part of the story. An alternative explanation could be that anti-retroviral treatment reduces viral load and allows LCs to function normally. Targeting LCs may be an alternative strategy worth considering, particularly in HIV-associated psoriasis, which can be notoriously difficult to treat. Indeed, LC inhibition may already be part of the success of UV phototherapy, one of the central treatments in ISDs, and a frontline treatment for HIV-associated cutaneous diseases, including both paradoxical

psoriasis and PPE. Depletion or alteration of LCs is a known effect of phototherapy (Bacci et al., 1998; Seite et al., 2003). This kind of therapy has also been shown to have considerable clinical effectiveness in treating not only psoriasis but also eczema and lichen planus (Jarrett and Scragg, 2017; Vangipuram and Feldman, 2016), both of which feature aberrant keratinocyte cell death (Devi et al., 2014; Gueiros et al., 2012; Sagari et al., 2016; Tobon-Aroyave et al., 2004; Trautmann et al., 2000). Accumulation of LCs has been observed in lichen planus (Devi et al., 2014; Gueiros et al., 2012), and in psoriasis, LCs appear to have an altered localization from the basal layer to the upper epidermis (Lowe et al., 2014). We similarly noted LCs localizing to the upper epidermis in *Sharpin*^{cpdm} skin. Perhaps LCs play an inflammatory, potentially death-inducing role in those conditions, contributing to overall pathogenesis.

With this work, we have shown a role for LCs in promoting the TNF-dependent inflammation in a mouse model of chronic ISD. The dermatitis phenotype is T cell independent, though functional T_{regs} can restrict inflammation. Replacement of *Sharpin*^{cpdm} LCs with *Sharpin*^{wt} LCs ameliorates inflammation even in the absence of mature T cell populations. Thus, whatever role *Sharpin*^{cpdm} LCs play in worsening the condition appears to be very different from their better-understood immunoregulatory roles involving activation and promotion of proliferation of T cell populations. The presence of *Sharpin*^{cpdm} LCs is associated with keratinocyte death and, ultimately, the development of dermatological disease. Importantly, replacement of *Sharpin*^{cpdm} LCs with *Sharpin*^{cpdm}*Tnf*^{-/-} LCs also prevents disease. These results suggest that LCs are an important cellular source of pathogenic TNF in *Sharpin*^{cpdm} mice and that they are capable of directly promoting inflammation in the skin, making them an attractive potential target for the treatment of dermatological disease.

Limitations of the study

Small n values were used in Figure 1, where we identified enriched immune-cell populations in the *Sharpin*^{cpdm} skin. Because no meaningful statistical analysis can be done with n = 3, we did not include p values. Results from Figure 1 were used to guide our further investigations but should not be interpreted as a comprehensive characterization of the *Sharpin*^{cpdm} immune infiltrate. That said, the LC increase seen in 3 *Sharpin*^{cpdm} mice in Figure 1 was also observed in 6 more mice in Figure 6.

DT treatment in the *Sharpin*^{cpdm}*Cd11b*^{DTR} mice did not deplete CD11b-expressing cells in the skin despite successfully depleting circulating CD11b cells. The specific reason for this is unclear: it could be that the dose of DT was insufficient to ensure

Figure 7. Transplantation of WT or *Sharpin*^{cpdm}*Tnf*^{-/-} bone marrow into langerin-depleted *Sharpin*^{cpdm} mice prevents dermatitis

(A) Outline of the LC depletion and bone marrow transplant experiments. DT depletes DTR expressing LCs, and irradiation depletes the rest of the haematopoietic system; donor LCs then repopulate the LC niche unless they also express DTR.
 (B) Clinical scoring of dermatitis. Twice weekly DT started at 3 weeks old and continued throughout the experiment until collection. Bone marrow transplant (BMT) performed when indicated. Graph shows mean ± SEM.
 (C) Representative images of transplanted animals as indicated at 7 weeks post-transplant.
 (D) Representative langerin staining of dorsal cross-sections from transplanted mice, plus an un-transplanted WT for reference. Scale bars, 50 μm. Dotted lines indicate the separation between epidermis and dermis.
 (E) Co-staining of dorsal sections for langerin and GFP in UBC-GFP and for langerin and CD45.1 in *Rag1*^{-/-} transplanted *Sharpin*^{cpdm}*Lang*^{DTR} mice. Scale bars, 50 μm.
 (F) H&E and IHC analysis of dorsal skin from the indicated transplants at 7 weeks post-transplant. Scale bars, 100 μm.
 See also Figure S7.

deletion of cells in the periphery. Regardless of the explanation, our results indicate that circulating CD11b cells are unimportant; however, no conclusion can be drawn as to the role of skin localized CD11b⁺ cells in the dermatitis phenotype.

Similarly, even though LCs express CCR2, we only observed partial protection from disease upon CCR2 deletion, and we were not able to confirm if skin localized CCR2⁺ cells were being depleted. We could not find evidence for acute depletion of LCs following DT treatment in *Sharpin^{cpdm}Ccr2^{DTR}* mice as assayed by epidermal ear sheet staining. One consideration is that CCR2⁺ monocytes will infiltrate and differentiate into LCs when activated LCs traffic out (Chopin and Nutt, 2015; Ginhoux and Merad, 2010; Kaplan, 2017). While our flow-cytometry data suggests that most of the LC increase in *Sharpin^{cpdm}* mice is due to local proliferation, the BM transplant experiment where we put *Sharpin* mutant marrow into LC-depleted *Sharpin^{cpdm}* mice shows that haematopoietically derived LCs can induce disease. The incomplete protection afforded by CCR2 depletion might be due to an indirect reduction in LCs in these mice that would not be apparent in the ear sheets following acute depletion; however, this is speculation only, and we have not shown any data to support this.

While our BM transplant data shows that TNF-expressing *Sharpin^{cpdm}* LCs are required to drive disease, implying that LCs are the cellular source of TNF, we have not been able to directly show increased expression of TNF by the mutant LCs *in vivo*. The potency of TNF as a cytokine means a slight increase in TNF can have big consequences; unfortunately, these changes appear to be below the detection limits of our current assays.

STAR★METHODS

Detailed methods are provided in the online version of this paper and include the following:

- KEY RESOURCES TABLE
- RESOURCE AVAILABILITY
 - Lead contact
 - Materials availability
 - Data and code availability
- EXPERIMENTAL MODEL AND SUBJECT DETAILS
 - Mice
 - Endemic pasturella at the WEHI
 - Allocation to experimental groups and gender balance
- METHOD DETAILS
 - Clinical scoring of chronic proliferative dermatitis (CPD) in SHARPIN deficient mice
 - Diphtheria toxin receptor (DTR) transgenic model
 - Bone marrow transplant experiments
 - Live *in vivo* multiphoton imaging
 - Preparation and imaging of whole skin mounts
 - Preparation of skin for flow cytometry analysis
 - Preparation of full-thickness skin samples for ELISA
 - Histology and immunofluorescence
 - IHC quantification
 - Preparation and imaging of epidermal ear sheets
- QUANTIFICATION AND STATISTICAL ANALYSIS

SUPPLEMENTAL INFORMATION

Supplemental information can be found online at <https://doi.org/10.1016/j.celrep.2022.110922>.

ACKNOWLEDGMENTS

We thank the staff of the WEHI Bioservices and histology facilities for practical assistance. This work was funded by NHMRC grants 1046984 (J.S., 2013–2016), 1105023 (J.S. 2016–2018), and 1155342 (S.L.N.), fellowships 1058190 (J.S., 2014–2018), 1107149 (J.S., 2016–2020), and 1194144 (H.A., 2020–2022), and scholarship 1093637 (H.A., 2015–2018); Australian Government Research Training Program Scholarships (H.A. and C.A.D.); the Jenny Thatchell/Pauline Speedy and the Barbara McDonald Innovation grants (M.C.); and donations from George Janko & Karen Inge Foundation and Thomas William Francis and Violet Coles Trust and was made possible through Victorian State Government Operational Infrastructure Support and Australian Government NHMRC IRIISS (GNT9000719).

AUTHOR CONTRIBUTIONS

Conceptualization, H.A., J.S., and N.L.; methodology, H.A., M.C., and C.A.D.; investigation, H.A., M.C., C.A.D., N.S., and L.W.; visualization, H.A., M.C., and C.A.D.; resources, J.S. and S.L.N.; funding acquisition, J.S., H.A., and S.L.N.; writing – original draft, H.A.; writing – review & editing, H.A., J.S., N.L., M.C., C.A.D., and S.L.N.; supervision, J.S. and N.L.

DECLARATION OF INTERESTS

The authors claim no competing interests.

INCLUSION AND DIVERSITY

One or more of the authors of this paper self-identifies as living with a disability. While citing references scientifically relevant for this work, we also actively worked to promote gender balance in our reference list.

Received: February 4, 2021

Revised: April 11, 2022

Accepted: May 17, 2022

Published: June 7, 2022

REFERENCES

- Aggarwal, B.B. (2003). Signalling pathways of the TNF superfamily: a double-edged sword. *Nat. Rev. Immunol.* 3, 745–756. <https://doi.org/10.1038/nri1184>.
- Akpinar Kara, Y. (2017). The measurement of serum TNF- α levels in patients with lichen planus. *Acta Dermatovenerol. Alp. Pannonica Adriat.* 26. <https://doi.org/10.15570/actaapa.2017.26>.
- Alpalhão, M., Borges-Costa, J., and Filipe, P. (2019). Psoriasis in HIV infection: an update. *Int. J. STD AIDS* 30, 596–604. <https://doi.org/10.1177/0956462419827673>.
- Altman, K., Vanness, E., and Westergaard, R.P. (2015). Cutaneous manifestations of human immunodeficiency virus: a clinical update. *Curr. Infect. Dis. Rep.* 17, 464. <https://doi.org/10.1007/s11908-015-0464-y>.
- Anderton, H., Rickard, J.A., Varigos, G.A., Lalaoui, N., and Silke, J. (2017). Inhibitor of apoptosis proteins (IAPs) limit RIPK1-mediated skin inflammation. *J. Invest. Dermatol.* 137, 2371–2379. <https://doi.org/10.1016/j.jid.2017.05.031>.
- Bacci, S., Romagnoli, P., and Wayne Streilein, J. (1998). Reduction in number and morphologic alterations of Langerhans cells after UVB radiation *in vivo* are accompanied by an influx of monocytoid cells into the epidermis. *J. Invest. Dermatol.* 111, 1134–1139. <https://doi.org/10.1046/j.1523-1747.1998.00406.x>.

- Bashir, M.M., Sharma, M.R., and Werth, V.P. (2009). TNF- α production in the skin. *Arch. Dermatol. Res.* *301*, 87–91. <https://doi.org/10.1007/s00403-008-0893-7>.
- Bennett, C.L., and Clausen, B.E. (2007). DC ablation in mice: promises, pitfalls, and challenges. *Trends Immunol.* *28*, 525–531. <https://doi.org/10.1016/j.it.2007.08.011>.
- Bennett, C.L., van Rijn, E., Jung, S., Inaba, K., Steinman, R.M., Kapsenberg, M.L., and Clausen, B.E. (2005). Inducible ablation of mouse Langerhans cells diminishes but fails to abrogate contact hypersensitivity. *J. Cell Biol.* *169*, 569–576. <https://doi.org/10.1083/jcb.200501071>.
- Berger, S.B., Kasparcova, V., Hoffman, S., Swift, B., Dare, L., Schaeffer, M., Capriotti, C., Cook, M., Finger, J., Hughes-Earle, A., et al. (2014). Cutting Edge: RIP1 kinase activity is dispensable for normal development but is a key regulator of inflammation in SHARPIN-deficient mice. *J. Immunol.* *192*, 5476–5480. <https://doi.org/10.4049/jimmunol.1400499>.
- Boisson, B., Laplantine, E., Dobbs, K., Cobat, A., Tarantino, N., Hazen, M., Lidov, H.G.W., Hopkins, G., Du, L., Belkadi, A., et al. (2015). Human HOIP and LUBAC deficiency underlies autoinflammation, immunodeficiency, amylopectinosis, and lymphangiectasia. *J. Exp. Med.* *212*, 939–951. <https://doi.org/10.1084/jem.20141130>.
- Boisson, B., Laplantine, E., Prando, C., Giliani, S., Israelsson, E., Xu, Z., Abhyankar, A., Israël, L., Trevejo-Nunez, G., Bogunovic, D., et al. (2012). Immunodeficiency, auto-inflammation and amylopectinosis in humans with inherited HOIL-1 and LUBAC deficiency. *Nat. Immunol.* *13*, 1178–1186. <https://doi.org/10.1038/ni.2457>.
- Cailhier, J.F., Partolina, M., Vuthoori, S., Wu, S., Ko, K., Watson, S., Savill, J., Hughes, J., and Lang, R.A. (2005). Conditional macrophage ablation demonstrates that resident macrophages initiate acute peritoneal inflammation. *J. Immunol.* *174*, 2336–2342. <https://doi.org/10.4049/jimmunol.174.4.2336>.
- Caldarola, G., De Simone, C., Carbone, A., Tulli, A., Amerio, P., and Feliciani, C. (2009). TNF α and its Receptors in Psoriatic Skin, before and after Treatment with Etanercept. *Int. J. Immunopathol. Pharmacol.* *22*, 961–966. <https://doi.org/10.1177/039463200902200411>.
- Cedeno-Laurent, F., Gómez-Flores, M., Mendez, N., Ancer-Rodríguez, J., Bryant, J.L., Gaspari, A.A., and Trujillo, J.R. (2011). New insights into HIV-1-primary skin disorders. *J. Int. AIDS Soc.* *14*, 5. <https://doi.org/10.1186/1758-2652-14-5>.
- Chiricozzi, A., Romanelli, P., Volpe, E., Borsellino, G., and Romanelli, M. (2018). Scanning the Immunopathogenesis of Psoriasis. *Int. J. Mol. Sci.* *19*, 179. <https://doi.org/10.3390/ijms19010179>.
- Chopin, M., and Nutt, S.L. (2015). Establishing and maintaining the Langerhans cell network. *Semin. Cell Dev. Biol.* *41*, 23–29. <https://doi.org/10.1016/j.semcdb.2014.02.001>.
- Cohen, J.A., Wu, J., and Kaplan, D.H. (2020). Neuronal regulation of cutaneous immunity. *J. Immunol.* *204*, 264–270. <https://doi.org/10.4049/jimmunol.1901109>.
- Cui, S., Xiao, T., Wang, Y., Lu, H., Wang, Y., Gao, X.-H., Wei, H., and Chen, H.-D. (2009). Morphological relationship between nerve fibers and Langerhans cells in the epidermis of psoriasis vulgaris and lichen simplex chronicus. *J. Dermatol. Sci.* *56*, 132–134. <https://doi.org/10.1016/j.jdermsci.2009.07.009>.
- Dawson, C.A., Pal, B., Vaillant, F., Gandolfo, L.C., Liu, Z., Blierot, C., Ginhoux, F., Smyth, G.K., Lindeman, G.J., Mueller, S.N., et al. (2020). Tissue-resident ductal macrophages survey the mammary epithelium and facilitate tissue remodelling. *Nat. Cell Biol.* *22*, 546–558. <https://doi.org/10.1038/s41556-020-0505-0>.
- Demehri, S., Liu, Z., Lee, J., Lin, M.-H., Crosby, S.D., Roberts, C.J., Grigsby, P.W., Miner, J.H., Farr, A.G., and Kopan, R. (2008). Notch-deficient skin induces a lethal systemic B-Lymphoproliferative disorder by secreting TSLP, a sentinel for epidermal integrity. *PLOS Biol.* *6*, e123. <https://doi.org/10.1371/journal.pbio.0060123>.
- Devi, M., Saraswathi, T.R., Ranganathan, K., Vijayalakshmi, D., Sreeja, C., and Fathima, S.S. (2014). Langerhans cells in lichen planus and lichenoid mucositis an immunohistochemical study. *J. Pharm. BioAllied Sci.* *6*, S146–S149. <https://doi.org/10.4103/0975-7406.137427>.
- Dogra, S., Bishnoi, A., Narang, T., and Handa, S. (2019). Secukinumab-induced paradoxical pustular psoriasis. *Clin. Exp. Dermatol.* *44*, 72–73. <https://doi.org/10.1111/ced.13731>.
- Doss, A.L.N., and Smith, P.G. (2014). Langerhans cells regulate cutaneous innervation density and mechanical sensitivity in mouse footpad. *Neurosci. Lett.* *578*, 55–60. <https://doi.org/10.1016/j.neulet.2014.06.036>.
- Eidsmo, L., and Martini, E. (2018). Human Langerhans cells with pro-inflammatory features relocate within psoriasis lesions. *Front. Immunol.* *9*, 300. <https://doi.org/10.3389/fimmu.2018.00300>.
- Ekpe, O. (2019). Pruritic papular eruption of HIV: a review article. *Our Dermatol. Online* *10*, 191–196. <https://doi.org/10.7241/ourd.20192.22>.
- Geissmann, F., Jung, S., and Littman, D.R. (2003). Blood monocytes consist of two principal subsets with distinct migratory properties. *Immunity* *19*, 71–82. [https://doi.org/10.1016/S1074-7613\(03\)00174-2](https://doi.org/10.1016/S1074-7613(03)00174-2).
- Gerlach, B., Cordier, S.M., Schmukle, A.C., Emmerich, C.H., Rieser, E., Haas, T.L., Webb, A.I., Rickard, J.A., Anderton, H., Wong, W.W.L., et al. (2011). Linear ubiquitination prevents inflammation and regulates immune signalling. *Nature* *471*, 591–596. <https://doi.org/10.1038/nature09816>.
- Gijbels, M.J., HogenEsch, H., Bruijzeel, P.L., Elliott, G.R., and Zurcher, C. (1995). Maintenance of donor phenotype After full-thickness skin transplantation from mice with chronic proliferative dermatitis (cpdm/dpdm) to C57BL/Ka and nude mice and vice versa. *J. Invest. Dermatol.* *105*, 769–773. <https://doi.org/10.1111/1523-1747.ep12325599>.
- Ginhoux, F., and Merad, M. (2010). Ontogeny and homeostasis of Langerhans cells. *Immunol. Cell Biol.* *88*, 387–392. <https://doi.org/10.1038/icb.2010.38>.
- Gomez Perdiguerro, E., Klapproth, K., Schulz, C., Busch, K., Azzoni, E., Crozet, L., Garner, H., Trouillet, C., de Bruijn, M.F., Geissmann, F., and Rodewald, H.R. (2015). Tissue-resident macrophages originate from yolk-sac-derived erythromyeloid progenitors. *Nature* *518*, 547–551. <https://doi.org/10.1038/nature13989>.
- Greuter, T., Navarini, A., and Vavricka, S.R. (2017). Skin Manifestations of Inflammatory Bowel Disease. *Clin. Rev. Allergy Immunol.* *53*, 413–427. <https://doi.org/10.1007/s12016-017-8617-4>.
- Gueiros, L.A., Gondak, R., Jorge Junior, J., Coletta, R.D., Carvalho, A.d.A., Leao, J.C., de Almeida, O.P., and Vargas, P.A. (2012). Increased number of Langerhans cells in oral lichen planus and oral lichenoid lesions. *Oral Surg Oral Med Oral Pathol Oral Radiol* *113*, 661–666. <https://doi.org/10.1016/j.oooo.2011.12.008>.
- HogenEsch, H., Gijbels, M.J., Offerman, E., van Hooft, J., van Bekkum, D.W., and Zurcher, C. (1993). A spontaneous mutation characterized by chronic proliferative dermatitis in C57BL mice. *Am. J. Pathol.* *143*, 972–982.
- Hohl, T.M., Rivera, A., Lipuma, L., Gallegos, A., Shi, C., Mack, M., and Pamer, E.G. (2009). Inflammatory monocytes facilitate adaptive CD4 T cell responses during respiratory fungal infection. *Cell Host Microbe* *6*, 470–481. <https://doi.org/10.1016/j.chom.2009.10.007>.
- Ikeda, F., Deribe, Y.L., Skanland, S.S., Stieglitz, B., Grabbe, C., Franz-Wachtel, M., van Wijk, S.J.L., Goswami, P., Nagy, V., Terzic, J., et al. (2011). SHARPIN forms a linear ubiquitin ligase complex regulating NF- κ B activity and apoptosis. *Nature* *471*, 637–641. <https://doi.org/10.1038/nature09814>.
- Jarrett, P., and Scragg, R. (2017). A short history of phototherapy, vitamin D and skin disease. *Photochem. Photobiol. Sci.* *16*, 283–290. <https://doi.org/10.1039/c6pp00406g>.
- Jung, S., Unutmaz, D., Wong, P., Sano, G.I., De los Santos, K., Sparwasser, T., Wu, S., Vuthoori, S., Ko, K., Zavala, F., et al. (2002). *In vivo* depletion of CD11c⁺ dendritic cells abrogates priming of CD8⁺ T cells by exogenous cell-associated antigens. *Immunity* *17*, 211–220. [https://doi.org/10.1016/S1074-7613\(02\)00365-5](https://doi.org/10.1016/S1074-7613(02)00365-5).
- Kaplan, D.H. (2010). *In vivo* function of Langerhans cells and dermal dendritic cells. *Trends Immunol.* *31*, 446–451. <https://doi.org/10.1016/j.it.2010.08.006>.
- Kaplan, D.H. (2017). Ontogeny and function of murine epidermal Langerhans cells. *Nat. Immunol.* *18*, 1068–1075. <https://doi.org/10.1038/ni.3815>.

- Kitashima, D.Y., Kobayashi, T., Woodring, T., Idouchi, K., Doebel, T., Voisin, B., Adachi, T., Ouchi, T., Takahashi, H., Nishifuji, K., et al. (2018). Langerhans cells prevent autoimmunity via expansion of keratinocyte antigen-specific regulatory T cells. *EBioMedicine* 27, 293–303. <https://doi.org/10.1016/j.ebiom.2017.12.022>.
- Komori, T., Honda, T., Endo, Y., Kaku, Y., Otsuka, A., and Kabashima, K. (2017). Oral lichen planus associated with candidiasis during secukinumab treatment. *J. Dermatol.* 44, e60–e61. <https://doi.org/10.1111/1346-8138.13637>.
- Kumari, S., Redouane, Y., Lopez-Mosqueda, J., Shiraishi, R., Romanowska, M., Lutzmayer, S., Kuiper, J., Martinez, C., Dikic, I., Pasparakis, M., and Ikeda, F. (2014). Sharpin prevents skin inflammation by inhibiting TNFR1-induced keratinocyte apoptosis. *Elife* 3, e03422. <https://doi.org/10.7554/eLife.03422>.
- Lis, K., Kuzawska, O., and Balkowicz-Iskra, E. (2014). State of the art paper Tumor necrosis factor inhibitors – state of knowledge. *Arch. Med. Sci.* 6, 1175–1185. <https://doi.org/10.5114/aoms.2014.47827>.
- Lowes, M.A., Suárez-Fariñas, M., and Krueger, J.G. (2014). Immunology of psoriasis. *Annu. Rev. Immunol.* 32, 227–255. <https://doi.org/10.1146/annurev-immunol-032713-120225>.
- Maglie, R., Di Cesare, A., Lazzeri, L., Pescitelli, L., Ricceri, F., Vannucchi, M., Massi, D., and Prignano, F. (2018). Lichen planus triggered by CT-P13 and recurrence during secukinumab treatment. *Br. J. Dermatol.* 178, 303–304. <https://doi.org/10.1111/bjd.16003>.
- Martini, E., Wiken, M., Cheuk, S., Gallais Serezal, I., Baharom, F., Stahle, M., Smed-Sorensen, A., and Eidsmo, L. (2017). Dynamic changes in resident and infiltrating epidermal dendritic cells in active and resolved psoriasis. *J. Invest. Dermatol.* 137, 865–873. <https://doi.org/10.1016/j.jid.2016.11.033>.
- Matsuzawa, T., Ogawa, Y., Moriishi, K., Shimada, S., and Kawamura, T. (2017). Immunological function of Langerhans cells in HIV infection. *J. Dermatol. Sci.* 87, 159–167. <https://doi.org/10.1016/j.jdermsci.2017.03.015>.
- Mayr, L., Su, B., and Moog, C. (2017). Langerhans cells: the “Yin and Yang” of HIV restriction and transmission. *Trends Microbiol.* 25, 170–172. <https://doi.org/10.1016/j.tim.2017.01.009>.
- Merad, M., Ginhoux, F., and Collin, M. (2008). Origin, homeostasis and function of Langerhans cells and other langerin-expressing dendritic cells. *Nat. Rev. Immunol.* 8, 935–947. <https://doi.org/10.1038/nri2455>.
- Merad, M., Manz, M.G., Karsunky, H., Wagers, A., Peters, W., Charo, I., Weissman, I.L., Cyster, J.G., and Engleman, E.G. (2002). Langerhans cells renew in the skin throughout life under steady-state conditions. *Nat. Immunol.* 3, 1135–1141. <https://doi.org/10.1038/nri852>.
- Mombaerts, P., Iacomini, J., Johnson, R.S., Herrup, K., Tonegawa, S., and Paupiano, V.E. (1992). RAG-1-deficient mice have no mature B and T lymphocytes. *Cell* 68, 869–877. [https://doi.org/10.1016/0092-8674\(92\)90030-G](https://doi.org/10.1016/0092-8674(92)90030-G).
- Morar, N., Willis-Owen, S.A., Maurer, T., and Bunker, C.B. (2010). HIV-associated psoriasis: pathogenesis, clinical features, and management. *Lancet Infect. Dis.* 10, 470–478. [https://doi.org/10.1016/S1473-3099\(10\)70101-8](https://doi.org/10.1016/S1473-3099(10)70101-8).
- Mössner, R., and Pinter, A. (2020). Paradoxical palmoplantar pustulosis induced by secukinumab and brodalumab: a report of three cases. *Eur. J. Dermatol.* 30, 177–178. <https://doi.org/10.1684/ejd.2020.3702>.
- Müller, K., and Meineke, V. (2007). Radiation-induced alterations in cytokine production by skin cells. *Exp. Hematol.* 35, 96–104. <https://doi.org/10.1016/j.exphem.2007.01.017>.
- Nagao, K., Ginhoux, F., Leitner, W.W., Motegi, S.I., Bennett, C.L., Clausen, B.E., Merad, M., and Udey, M.C. (2009). Murine epidermal Langerhans cells and langerin-expressing dermal dendritic cells are unrelated and exhibit distinct functions. *Proc. Natl. Acad. Sci. U S A* 106, 3312–3317. <https://doi.org/10.1073/pnas.0807126106>.
- Namazi, M.R. (2004). Paradoxical exacerbation of psoriasis in AIDS: proposed explanations including the potential roles of substance P and gram-negative bacteria. *Autoimmunity* 37, 67–71. <https://doi.org/10.1080/08916930310001637986>.
- Navarro-Triviño, F.J., Sanchez-Parera, R., and Ruiz-Villaverde, R. (2020). Secukinumab-induced paradoxical hidradenitis suppurativa. *Dermatol. Ther.* 33, e13150. <https://doi.org/10.1111/dth.13150>.
- Noell, C., McQuade, B., Gottlieb, A., and Rosmarin, D. (2017). Anti IL-17 flared psoriasis in a patient on secukinumab. *Dermatol. Ther.* 30, e12505. <https://doi.org/10.1111/dth.12505>.
- Oda, H., Beck, D.B., Kuehn, H.S., Sampaio Moura, N., Hoffmann, P., Ibarra, M., Stoddard, J., Tsai, W.L., Gutierrez-Cruz, G., Gadina, M., et al. (2019). Second Case of HOIP Deficiency Expands Clinical Features and Defines Inflammatory Transcriptome Regulated by LUBAC. *Front. Immunol.* 10. <https://doi.org/10.3389/fimmu.2019.00479>.
- Ostrowski, S.M., Belkadi, A., Loyd, C.M., Diaconu, D., and Ward, N.L. (2011). Cutaneous denervation of psoriasiform mouse skin improves acanthosis and inflammation in a sensory neuropeptide-dependent manner. *J. Invest. Dermatol.* 137, 1530–1538. <https://doi.org/10.1038/jid.2011.60>.
- Park, Y., Jin, H.s., Lopez, J., Lee, J., Liao, L., Elly, C., and Liu, Y.-C. (2016). SHARPIN controls regulatory T cells by negatively modulating the T cell antigen receptor complex. *Nat. Immunol.* 17, 286–296. <https://doi.org/10.1038/ni.3352>.
- Petrof, G., Almaani, N., Archer, C.B., Griffiths, W. a. D., and Smith, C.H. (2013). A systematic review of the literature on the treatment of pityriasis rubra pilaris type 1 with TNF-antagonists. *J. Eur. Acad. Dermatol. Venereol.* 27, e131–e135. <https://doi.org/10.1111/j.1468-3083.2012.04456.x>.
- Potter, C.S., Wang, Z., Silva, K.A., Kennedy, V.E., Stearns, T.M., Burzenski, L., Shultz, L.D., Hogenesch, H., and Sundberg, J.P. (2014). Chronic proliferative dermatitis in Sharpin null mice: development of an autoinflammatory disease in the absence of B and T lymphocytes and IL4/IL13 signaling. *PLoS One* 9, e85666. <https://doi.org/10.1371/journal.pone.0085666>.
- Redecke, V., Chaturvedi, V., Kuriakose, J., and Häcker, H. (2016). SHARPIN controls the development of regulatory T cells. *Immunology* 148, 216–226. <https://doi.org/10.1111/imm.12604>.
- Renninger, M.L., Seymour, R.E., Whiteley, L.O., Sundberg, J.P., and Hogenesch, H. (2010). Anti-IL5 decreases the number of eosinophils but not the severity of dermatitis in Sharpin-deficient mice. *Exp. Dermatol.* 19, 252–258. <https://doi.org/10.1111/j.1600-0625.2009.00944.x>.
- Rickard, J.A., Anderton, H., Etemadi, N., Nachbur, U., Darding, M., Peltzer, N., Lalaoui, N., Lawlor, K.E., Vanyai, H., Hall, C., et al. (2014). TNFR1-dependent cell death drives inflammation in Sharpin-deficient mice. *Elife* 3, 1–23. <https://doi.org/10.7554/eLife.03464>.
- Rios, A.C., Capaldo, B.D., Vaillant, F., Pal, B., van Ineveld, R., Dawson, C.A., Chen, Y., Nolan, E., Fu, N.Y., Jackling, F.C., et al. (2019). Intracanal plasticity in mammary tumors revealed through large-scale single-cell resolution 3D imaging. *Cancer Cell* 35, 618–632.e6. <https://doi.org/10.1016/j.ccell.2019.02.010>.
- Sagari, S., Sanadhya, S., Doddamani, M., and Rajput, R. (2016). Molecular markers in oral lichen planus: a systematic review. *J. Oral Maxillofac. Pathol.* 20, 115–121. <https://doi.org/10.4103/0973-029X.180964>.
- Sasaki, K., Himeno, A., Nakagawa, T., Sasaki, Y., Kiyonari, H., and Iwai, K. (2019). Modulation of autoimmune pathogenesis by T cell-triggered inflammatory cell death. *Nat. Commun.* 10, 3878. <https://doi.org/10.1038/s41467-019-11858-7>.
- Schaefer, B.C., Schaefer, M.L., Kappler, J.W., Marrack, P., and Kedl, R.M. (2001). Observation of antigen-dependent CD8+ T-cell/ dendritic cell interactions *in vivo*. *Cell. Immunol.* 214, 110–122. <https://doi.org/10.1006/cimm.2001.1895>.
- Schindelin, J., Arganda-Carreras, I., Frise, E., Kaynig, V., Longair, M., Pietzsch, T., Preibisch, S., Rueden, C., Saalfeld, S., Schmid, B., et al. (2012). Fiji: an open-source platform for biological-image analysis. *Nat. Methods* 9, 676–682. <https://doi.org/10.1038/nmeth.2019>.
- Seite, S., Zucchi, H., Moyal, D., Tison, S., Compan, D., Christiaens, F., Gueniche, A., and Fourtanier, A. (2003). Alterations in human epidermal Langerhans cells by ultraviolet radiation: quantitative and morphological study. *Br.*

- J. Dermatol. 148, 291–299. <https://doi.org/10.1046/j.1365-2133.2003.05112.x>.
- Seneschal, J., Clark, R.A., Gehad, A., Baecher-Allan, C.M., and Kupper, T.S. (2012). Human epidermal Langerhans cells maintain immune homeostasis in skin by activating skin resident regulatory T cells. *Immunity* 36, 873–884. <https://doi.org/10.1016/j.immuni.2012.03.018>.
- Singh, T.P., Zhang, H.H., Borek, I., Wolf, P., Hedrick, M.N., Singh, S.P., Kelsall, B.L., Clausen, B.E., and Farber, J.M. (2016). Monocyte-derived inflammatory Langerhans cells and dermal dendritic cells mediate psoriasis-like inflammation. *Nat. Commun.* 7, 13581. <https://doi.org/10.1038/ncomms13581>.
- Speeckaert, R., Lambert, J., and van Geel, N. (2019). Learning From Success and Failure: Biologics for Non-approved Skin Diseases. *Front. Immunol.* 10. <https://doi.org/10.3389/fimmu.2019.01918>.
- Sweeney, C.M., Russell, S.E., Malara, A., Kelly, G., Hughes, R., Tobin, A.M., Adamzik, K., Walsh, P.T., and Kirby, B. (2016). Human β -defensin 3 and its mouse ortholog murine β -defensin 14 activate Langerhans cells and exacerbate psoriasis-like skin inflammation in mice. *J. Invest. Dermatol.* 136, 723–727. <https://doi.org/10.1016/j.jid.2015.12.011>.
- Teh, C.E., Lalaoui, N., Jain, R., Policheni, A.N., Heinlein, M., Alvarez-Diaz, S., Sheridan, J.M., Rieser, E., Deuser, S., Darding, M., et al. (2016). Linear ubiquitin chain assembly complex coordinates late thymic T-cell differentiation and regulatory T-cell homeostasis. *Nat. Commun.* 7, 13353. <https://doi.org/10.1038/ncomms13353>.
- Terhorst, D., Chelbi, R., Wohn, C., Malosse, C., Tamoutounour, S., Jorquera, A., Bajenoff, M., Dalod, M., Malissen, B., and Henri, S. (2015). Dynamics and transcriptomics of skin dendritic cells and macrophages in an imiquimod-induced, biphasic mouse model of psoriasis. *J. Immunol.* 195, 4953–4961. <https://doi.org/10.4049/jimmunol.1500551>.
- Thompson, J.M., Cohen, L.M., Yang, C.S., and Kroumpouzos, G. (2016). Severe, ulcerative, lichenoid mucositis associated with secukinumab. *JAAD Case Rep.* 2, 384–386. <https://doi.org/10.1016/j.jdc.2016.07.009>.
- Tobon-Arroyave, S.I., Villegas-Acosta, F.A., Ruiz-Restrepo, S.M., Vieco-Duran, B., Restrepo-Misas, M., and Londono-Lopez, M.L. (2004). Expression of caspase-3 and structural changes associated with apoptotic cell death of keratinocytes in oral lichen planus. *Oral Dis.* 10, 173–178. <https://doi.org/10.1046/j.1601-0825.2003.00998.x>.
- Tokunaga, F., Nakagawa, T., Nakahara, M., Saeki, Y., Taniguchi, M., Sakata, S.i., Tanaka, K., Nakano, H., and Iwai, K. (2011). SHARPIN is a component of the NF- κ B-activating linear ubiquitin chain assembly complex. *Nature* 471, 633–636. <https://doi.org/10.1038/nature09815>.
- Tracey, D., Klareskog, L., Sasso, E.H., Salfeld, J.G., and Tak, P.P. (2008). Tumor necrosis factor antagonist mechanisms of action: a comprehensive review. *Pharmacol. Ther.* 117, 244–279. <https://doi.org/10.1016/j.pharmthera.2007.10.001>.
- Trautmann, A., Akdis, M., Kleemann, D., Altnauer, F., Simon, H.U., Graeve, T., Noll, M., Brocker, E.B., Blaser, K., and Akdis, C.A. (2000). T cell-mediated Fas-induced keratinocyte apoptosis plays a key pathogenetic role in eczematous dermatitis. *J. Clin. Invest.* 106, 25–35. <https://doi.org/10.1172/JCI9199>.
- Tsou, C.-L., Peters, W., Si, Y., Slaymaker, S., Aslanian, A.M., Weisberg, S.P., Mack, M., and Charo, I.F. (2007). Critical roles for CCR2 and MCP-3 in monocyte mobilization from bone marrow and recruitment to inflammatory sites. *J. Clin. Invest.* 117, 902–909. <https://doi.org/10.1172/JCI29919>.
- van der Aar, A.M., Picavet, D.I., Muller, F.J., de Boer, L., van Capel, T.M., Zaat, S.A., Bos, J.D., Janssen, H., George, T.C., Kapsenberg, M.L., et al. (2013). Langerhans cells favor skin flora tolerance through limited presentation of bacterial antigens and induction of regulatory T cells. *J. Invest. Dermatol.* 133, 1240–1249. <https://doi.org/10.1038/jid.2012.500>.
- Vangipuram, R., and Feldman, S.R. (2016). Ultraviolet phototherapy for cutaneous diseases: a concise review. *Oral Dis.* 22, 253–259. <https://doi.org/10.1111/odi.12366>.
- Wang, Z., Sokolovska, A., Seymour, R., Sundberg, J.P., and Hogenesch, H. (2012). SHARPIN is essential for cytokine production, NF- κ B signaling, and induction of Th1 differentiation by dendritic cells. *PLoS One* 7, e31809. <https://doi.org/10.1371/journal.pone.0031809>.
- West, H.C., and Bennett, C.L. (2017). Redefining the role of Langerhans cells as immune regulators within the skin. *Front. Immunol.* 8, 1941. <https://doi.org/10.3389/fimmu.2017.01941>.
- Xiao, C., Zhu, Z., Sun, S., Gao, J., Fu, M., Liu, Y., Wang, G., Yao, X., and Li, W. (2017). Activation of Langerhans cells promotes the inflammation in imiquimod-induced psoriasis-like dermatitis. *J. Dermatol. Sci.* 85, 170–177. <https://doi.org/10.1016/j.jdermsci.2016.12.003>.
- Zaba, L.C., Cardinale, I., Gilleaudeau, P., Sullivan-Whalen, M., Suárez-Fariñas, M., Fuentes-Duculan, J., Novitskaya, I., Khatcharian, A., Bluth, M.J., Lowes, M.A., and Krueger, J.G. (2007). Amelioration of epidermal hyperplasia by TNF inhibition is associated with reduced Th17 responses. *J. Exp. Med.* 204, 3183–3194. <https://doi.org/10.1084/jem.20071094>.
- Zak, D.E., Schmitz, F., Gold, E.S., Diercks, A.H., Peschon, J.J., Valvo, J.S., Niemisto, A., Podolsky, I., Fallen, S.G., Suen, R., et al. (2011). Systems analysis identifies an essential role for SHANK-associated RH domain-interacting protein (SHARPIN) in macrophage Toll-like receptor 2 (TLR2) responses. *Proc. Natl. Acad. Sci. U S A* 108, 11536–11541. <https://doi.org/10.1073/pnas.1107577108>.
- Zhan, Y., Zhang, Y., Zhang, S., Coughlan, H., Baldoni, P.L., Jacquolot, N., Cao, W.H.J., Preston, S., Louis, C., Rautela, J., et al. (2021). Differential requirement for the Polycomb repressor complex 2 in dendritic cell and tissue-resident myeloid cell homeostasis. *Sci. Immunol.* 6, eabf7268. <https://doi.org/10.1126/sciimmunol.abf7268>.
- Dowlatshahi, E.A., Voort, E.A.M. van der, Arends, L.R., Nijsten, T., 2013. Markers of systemic inflammation in psoriasis: a systematic review and meta-analysis. *Br. J. Dermatol.* 169, 266–282. <https://doi.org/10.1111/bjd.12355>
- Vossen, A.R.J.V., Ardon, C.B., Zee, H.H. van der, Lubberts, E., Prens, E.P., 2019. The anti-inflammatory potency of biologics targeting tumour necrosis factor- α , interleukin (IL)-17A, IL-12/23 and CD20 in hidradenitis suppurativa: an ex vivo study. *Br. J. Dermatol.* 181, 314–323. <https://doi.org/10.1111/bjd.17641>
- Zee, H.H. van der, Rüter, L. de, Broecke, D.G. van den, Dik, W.A., Laman, J.D., Prens, E.P., 2011. Elevated levels of tumour necrosis factor (TNF)- α , interleukin (IL)-1 β and IL-10 in hidradenitis suppurativa skin: a rationale for targeting TNF- α and IL-1 β . *Br. J. Dermatol.* 164, 1292–1298. <https://doi.org/10.1111/j.1365-2133.2011.10254.x>

STAR★METHODS

KEY RESOURCES TABLE

REAGENT or RESOURCE	SOURCE	IDENTIFIER
Antibodies		
goat anti-rat AF-594	Thermo Fisher Scientific	RRID: AB_10561522
Rabbit anti-Ki67 (SP6)	Thermo Fisher Scientific	RRID: AB_10979488
FITC Anti-mouse Ki-67 (SolA15)	eBioscience	RRID: AB_11151330
APC Anti-mouse CD326 (G8.8)	BioLegend	RRID: AB_1134105
goat anti-rabbit AF-488	Thermo Fisher Scientific	RRID: AB_143165
APC-CY7 Anti-mouse CD326 (G8.8)	BioLegend	RRID: AB_1501158
eFluor450 Anti-mouse CD11b (M1/70)	eBioscience	RRID: AB_1582236
APC-Cy7 Anti-mouse MHC II (M5)	BioLegend	RRID: AB_1659252
V450 Anti-mouse Ly6c (AL-21)	BD Biosciences	RRID: AB_1727559
Rat anti-mouse CD45	BD Biosciences	RRID: AB_2174426
Rabbit anti-GFP	Invitrogen	RRID: AB_221569
goat anti-mouse AF-488	Thermo Fisher Scientific	RRID: AB_2534069
Goat anti-rat AF-488	Invitrogen	RRID: AB_2534074
Donkey anti-rabbit AF-647	Invitrogen	RRID: AB_2536183
Brilliant Violet 785 Anti-mouse CD11b (M1/70)	BioLegend	RRID: AB_2561373
APC Anti-mouse CD207 (4C7)	BioLegend	RRID: AB_2561997
APC Anti-mouse XCR1 (ZET)	BioLegend	RRID: AB_2563931
Brilliant Violet 650 XCR1 (ZET)	BioLegend	RRID: AB_2566410
Brilliant Violet 605 Anti-mouse CD64 (X54-5/7.1)	BioLegend	RRID: AB_2629778
anti-PGP9.5 (Abcam, UK)	Abcam,	RRID: AB_27053
BUV 786 Anti-mouse CD45.2 (104)	BD Biosciences	RRID: AB_2738375
Brilliant Violet 650 Anti-mouse CD86 (GL1)	BD Biosciences	RRID: AB_2738665
BUV 395 Anti-mouse CD45.2 (104)	BD Biosciences	RRID: AB_2738867
BV 510 Anti-mouse MHCII (M5/114)	BD Biosciences	RRID: AB_2741133
anti-CD16/CD32 (2.4G2)	BD Biosciences	RRID: AB_394656
PE Anti-mouse TCR- $\gamma\delta$ (GL3)	BD Biosciences	RRID: AB_394689
FITC Anti-mouse MHC II (M5)	eBioscience	RRID: AB_465232
PE Anti-mouse CD40 (1C10)	Invitrogen	RRID: AB_465649
PE Anti-mouse MHC II (M5)	eBioscience	RRID: AB_465928
anti-CD45.1 (A20)	eBioscience	RRID: AB_467258
APC Anti-mouse TCRb (H57-597)	eBioscience	RRID: AB_469481
PeCy7 Anti-mouse CD11c (N418)	eBioscience	RRID: AB_469590
Rat anti-MHCII AF 647 clone M5/114	BioLegend	RRID: AB_493526
PerCP-Cy5.5 Anti-mouse Ly-6G/Ly-6C (RB6-8C5)	eBioscience	RRID: AB_906247
Brilliant Violet 711 Anti-mouse CD45.2 (104)	BioLegend	Cat# 109847
BUV 737 Anti-mouse CD80 (16-10A1)	BD Biosciences	Cat# 612773
Rabbit anti-CC3 clone 5A1E,	Cell Signalling Technologies	Cat# 9664
goat anti-rabbit biotinylated secondary	Vector Laboratories	Cat# BA-1000-1.5
Langerin/CD207 Antibody (310F7.02)	Novus Biologicals	Cat# DDX0361P
Rabbit anti-human CD3	Agilent Technologies	Cat# GA503
FITC Anti-mouse CD11c (N418)	WEHI antibody facility	n/a
Rabbit anti-F4/80	WEHI antibody facility	n/a

(Continued on next page)

Continued

REAGENT or RESOURCE	SOURCE	IDENTIFIER
Rat anti-MHCII clone M5/114,	WEHI antibody facility	n/a
Chemicals, peptides, and recombinant proteins		
Normal Goat Serum (NGS)	Invitrogen	RRID: AB_2532166
FUnGI clearing agent	(Rios et al., 2019)	n/a
Peroxidase-Blocking Solution, Dako Real	Agilent Technologies	Cat# S202386-2
Liquid DAB+, 2-component system, Immunohistochemistry Visualization,	Agilent Technologies	Cat# K346811-2
Dow Corning silicone high vacuum grease	ProSciTech	Cat# M020X
GIBCO DPBS	Thermo Fisher	Cat# 14190144
DAPI	Invitrogen	Cat# D1306
Gibco™ Dispase II, powder	Thermo Fisher	Cat# 17-105-041
Phalloidin-AF 555	Invitrogen	Cat# A-34055
Isoflurane	Novachem	Cat# 099-06571
Tissue-Tek optimal cutting temperature (OCT) embedding medium	ProSciTech	Cat# IA018
Liberase (Dispase High)	Roche	Cat# 5401054001
DNase I	Roche	Cat# 11284932001
cOmplete cocktail protease inhibitor (Roche)	Roche	Cat# 04693116001
Paraformaldehyde	Sigma-Aldrich	Cat# 158127
Diphtheria Toxin	Sigma-Aldrich	Cat# D0564
Triton X-100	Sigma-Aldrich	Cat# X100
Tween 20	Sigma-Aldrich	Cat# P1379
Bovine Serum Albumin (BSA)	Sigma-Aldrich	Cat# A7030
ethylene-diamine-tetra-acetic acid (EDTA)	Sigma-Aldrich	Cat# E8145
glycerol	Sigma-Aldrich	Cat# G5516
acetone	Sigma-Aldrich	Cat# 179124
xylene	Sigma-Aldrich	Cat# 534056
DPX mountant	Sigma-Aldrich	Cat# 06522
ammonium thiocyanate	Sigma-Aldrich	Cat# A7149
Sodium Azide	Sigma-Aldrich	Cat# S2002
propidium iodide	Thermo Fisher	Cat# P1304MP
Fluoromount-G mounting medium with DAPI	Thermo Fisher	Cat# 00-4959-52
Slowfade Diamond antifade mountant	Thermo Fisher	Cat# S36972
avidin-biotin blocking kit;	Vector Laboratories	Cat# SP-2001
VECTASTAIN Elite ABC HRP Kit	Vector Laboratories	Cat# PK-6100
Critical commercial assays		
TNF alpha Mouse ELISA kit	Invitrogen	Cat# 88-7324-88
Pierce™ BCA Protein Assay Kit	Thermo Fisher	Cat# 23225
Experimental models: Organisms/strains		
Mouse: Ly5.1.Rag1 ^{-/-} ; Rag1 ^{tm1Mom}	(Mombaerts et al., 1992)	IMSR_JAX:002216
Mouse: UBC-GFP: C57BL/6-Tg(UBC-GFP)30Scha/J	(Schaefer et al., 2001)	IMSR_JAX:004353
Mouse: CD11c-DTR (CD11c ^{DTR}): 1700016L21Rik ^{Tg(ttgax-DTR/EGFP)57Lan}	(Jung et al., 2002)	IMSR_JAX:004509
Mouse: CD11b-DTR (Cd11b ^{DTR}): Tg(ITGAM-DTR/EGFP)34Lan	(Cailhier et al., 2005)	IMSR_JAX:006000
Mouse: langerin-DTR (Langerin ^{DTR}): Cd207 ^{tm3.1(HBEGF/EGFP)Mal}	(Bennett et al., 2005)	IMSR_JAX:016940

(Continued on next page)

Continued

REAGENT or RESOURCE	SOURCE	IDENTIFIER
Mouse: <i>Sharpin</i> ^{cpdm} : C57BL/KaLawRij- <i>Sharpin</i> ^{cpdm}	(HogenEsch et al., 1993)	MGI:3695413
Mouse: <i>Sharpin</i> ^{cpdm} <i>Cd11b</i> ^{DTR}	This manuscript	Strain ID: B6.Sharpin(cpdm)
Mouse: <i>Sharpin</i> ^{cpdm} <i>Cd11c</i> ^{DTR}	This manuscript	Strain ID: B6.Sharpin(cpdm)
Mouse: <i>Sharpin</i> ^{cpdm} <i>Ccr2</i> ^{DTR}	This manuscript	Strain ID: B6.Sharpin(cpdm) CCR2-DTR
Mouse: <i>Sharpin</i> ^{cpdm} <i>Lang</i> ^{DTR}	This manuscript	Strain ID: B6.Sharpin(cpdm) Lg-DTR
Mouse: <i>Sharpin</i> ^{cpdm} <i>Suz12</i> ^{flox/flox} <i>Cd11c</i> ^{Cre}	This manuscript	Strain ID: B6.Sharpin(cpdm) Suz12creCD11C
Mouse: <i>Sharpin</i> ^{cpdm} <i>Tnf</i> ^{-/-}	(Gerlach et al. 2011)	Strain ID: B6.Sharpin(cpdm) TNFko
Mouse: CCR2-DTR (<i>Ccr2</i> ^{DTR}): CCR2.DTR.CFP	(Hohl et al., 2009)	Strain ID: CCR2.DTR.CFP
Mouse: <i>Suz12</i> ^{Cd11c} : <i>Suz12</i> ^{flox/flox} <i>Cd11c</i> ^{Cre}	(Zhan et al., 2021)	Strain ID: Suz12.CD11cCre

Software and algorithms

GraphPad Prism 9.3.1	GraphPad Software, LLC	https://www.graphpad.com/
FlowJo 10.8.1	FlowJo LLC	https://www.flowjo.com/
Fiji Image J	SciJava Ecosystem	https://fiji.sc
Imaris (Bitplane)	Oxford Instruments Group	https://imaris.oxinst.com/
cellSens imaging software	Olympus	https://www.olympus-lifescience.com/en/software/cellsens/powerful-analysis-tools/
SlideViewer	3D Histech	https://www.3dhitech.com/research/digital-microscopes-viewers/slideviewer/

RESOURCE AVAILABILITY

Lead contact

Further information and requests for resources and reagents should be directed to and will be fulfilled by the lead contact, John Silke (silke@wehi.edu.au).

Materials availability

Unique mouse lines generated in this study are available from the [lead contact](#) upon request with a completed Materials Transfer Agreement.

Data and code availability

- The datasets generated and/or analysed during the current study are available from the [lead contact](#), John Silke (silke@wehi.edu.au), upon reasonable request.
- This paper does not report original code.
- Any additional information required to reanalyze the data reported in this paper is available from the [lead contact](#) upon request

EXPERIMENTAL MODEL AND SUBJECT DETAILS

Mice

The WEHI Animal Ethics Committee approved all mouse experiments, which were conducted according to the Australian Code for the care and use of animals for scientific purposes. Established mouse strains used in this project and generated and housed at the Walter and Eliza Hall Institute of Medical Research (WEHI) Specified Pathogen Free (SPF) Bioservices facilities in Parkville (VIC) 3052 are *Sharpin*^{cpdm} (HogenEsch et al., 1993); *Sharpin*^{cpdm}*Tnf*^{-/-} (Gerlach et al., 2011); *CD11b*-DTR(*CD11b*^{DTR}) (Cailhier et al., 2005); CCR2-DTR (*Ccr2*^{DTR}) (Hohl et al., 2009); *CD11c*-DTR (*CD11c*^{DTR}) (Jung et al., 2002); *langerin*-DTR (*Lang*^{DTR}) (Bennett et al., 2005); *Suz12*^{flox/flox}*Cd11c*^{Cre} (*Suz12*^{Cd11c}ΔLC) (Zhan et al., 2021); UBC-GFP (Schaefer et al., 2001). *Ly5.1.Rag1*^{-/-} (Mombaerts et al., 1992) bone marrow donor mice were generated at the WEHI SPF Bioservices facilities in Kew (VIC) 3101. Unique mouse crosses generated specifically for this project and housed at the WEHI SPF Bioservices facilities in Parkville (VIC) 3052 are *Sharpin*^{cpdm}*Cd11b*^{DTR}; *Sharpin*^{cpdm}*Ccr2*^{DTR}; *Sharpin*^{cpdm}*Cd11c*^{DTR}; *Sharpin*^{cpdm}*Lang*^{DTR}; *Sharpin*^{cpdm}*Suz12*^{flox/flox}*Cd11c*^{Cre} (*Sharpin*^{cpdm}*Suz12*^{Cd11c}).

Germ-free *Sharpin*^{cpdm} mice were caesarean sectioned from an SPF mother at embryonic day 19 into the WEHI's germ-free facility at Kew (VIC) 3101 to germ-free foster mothers housed within positive pressure germ-free isolators. All strains are on a c57bl/6 background with a minimum of 5 generation backcross.

Endemic pasteurilla at the WEHI

The WEHI SPF facility at Parkville had endemic *Pasteurella* during the time the experiments were performed. While this infection was subclinical in immunocompetent mice many of the strains in this project had increased susceptibility to infection, which was further exacerbated upon DTR mediated depletion of some immune cell populations. Several mice were removed early from experiments due to infections resulting in pneumonia. This has been clearly indicated on graphs and in figure legends. To prevent emergence of clinical infection in DT treated mice that were also to undergo irradiation and bone marrow transplant (Figure 7), prophylactic Enrofloxacin (Baytril) was added to the drinking water and available ad libitum. A 400 mL hydropak with 4.1 mLs of a 50 mg/mL Baytril solution added was provided to breeders post-partum until litters were weaned. Ongoing prophylactic Baytril was provided to the weaned litters throughout DT treatment, irradiation and transplant. Antibiotic water was changed weekly.

Allocation to experimental groups and gender balance

Entire litters of mice were assigned to experimental groups at weaning (3 weeks old) prior to genotyping. Both male and female mice were used in all experiments. The number of each sex and genotype in each experimental group represents the proportion of each sex and genotype that were weaned at the time the experiment was performed. With the exception of body weight, the data presented in this manuscript is pooled male and female data.

METHOD DETAILS

Clinical scoring of chronic proliferative dermatitis (CPD) in SHARPIN deficient mice

We developed a 6-point ordinal scale (0-5) to track *Sharpin*^{cpdm} chronic proliferative dermatitis symptoms (Table 1). To minimise bias, animal technicians familiar with the phenotype and the scoring system performed all scoring. Littermate controls used throughout and referred to as Control (or con) include *Sharpin*^{wt/wt} and *Sharpin*^{cpdm/wt} because the heterozygotes are phenotypically identical to WT animals.

Diphtheria toxin receptor (DTR) transgenic model

Diphtheria Toxin (Sigma-Aldrich, Australia) treatment began when the mice were weaned at 21-24 days old. For the CD11b, CCR2 and langerin-DTR groups, mice were weighed, scored for *Sharpin*^{cpdm} phenotype, and 8 ng DT/g of body weight was injected intraperitoneally. Injections were performed twice weekly to maintain clearance of the target cell types. The *Cd11c*^{DTR} mice cannot tolerate multiple systemic doses of DT. In order to avoid systemic effects, these mice were instead administered DT locally. 100ul of 1 ng/ul DT was subcutaneously injected into the dorsal region twice weekly throughout the experimental period.

Bone marrow transplant experiments

Mice were treated with DT from weaning as per our typical protocol. At six weeks of age, the animals were irradiated and IV injected with either *Sharpin*^{cpdm} bone marrow (no DTR, positive controls), with UBC-GFP bone marrow (functionally WT, no DTR, transplanted cells express GFP), with *Sharpin*^{cpdm} *Lang*^{DTR} bone marrow (have DTR, negative controls), with *Ly5.1.Rag1*^{-/-} bone marrow (no DTR, *Sharpin*^{wt/wt}, unable to reconstitute mature B or T cells), or with *Sharpin*^{cpdm} *Tnf*^{-/-} bone marrow (no DTR, reconstituted cells will not express TNF). DT treatment continued throughout the experiment to ensure the host LC niche remained empty.

Live in vivo multiphoton imaging

Mice were anaesthetised with 3% isoflurane then 1-2% isoflurane in oxygen, and their temperature maintained at 37°C by a rectal probe and thermostatic heat pad. To enable imaging of LCs and apoptotic cells, 2.5 µg of MHCII Alexa Fluor 647 (rat, M5/114; BioLegend) and 2.5 µg propidium iodide (Thermo Fisher) in 10 µL were injected intradermally in the ear pinnae. The ear was secured to a raised platform, the injected area outlined with silicone grease (Dow Corning) and covered with Phosphate Buffered Saline (PBS, Gibco) then a coverslip was placed on top (Dawson et al., 2020). The coverslip was outlined with hydrophobic pen to contain objective immersion water. The mouse was placed in a 35°C microscope chamber, and hydration was maintained by hourly intraperitoneal injections of 6.25 µL/g saline. Images were acquired with an upright FVMP-RS multiphoton microscope (Olympus) with dual MaiTai DeepSee and InSight DeepSee lasers (Spectra-Physics), two GaAsP and two MultiAlkali photomultiplier tube detectors and an x25/1.05 NA water objective (Olympus). Three-dimensional image stacks were acquired at 512 x 512 pixels and 1.5x zoom with a 2 µm z-step every 5 min for up to 5 h, after which the mouse was euthanised by cervical dislocation. Alexa Fluor 647 was excited by 1,200 nm laser and collected through a 705/90 nm (centre/width) bandwidth filter (Semrock). Second-harmonic generation by collagen was stimulated by 950 nm laser and collected through a 450/70 nm band-pass filter (Semrock). Images were processed and analysed in Imaris (Bitplane). After manual movement correction, MHCII-high LCs were identified by epidermal location and dendritic morphology. Migration and density were measured by manually placing spots on the cell bodies, then measuring their average speed and distance from the nearest neighbour. The effect of image drift on migration measurements was removed by tracking collagen structures and subtracting the average drift speed from the LC measurements.

Preparation and imaging of whole skin mounts

Dorsal skin was shaved and cleared with Nair; then, the fat was gently scraped off with a scalpel. The skin was laid flat in histology cassettes and fixed in 4% PFA overnight at 4°C on an orbital shaker. Following steps at room temperature: the skin was placed in a 12-well plate and washed for 1 h with PBS, then permeabilised with 0.3% Triton X-100 (Sigma-Aldrich) in PBS for 5–8 h. Primary antibodies (rat anti-mouse MHCII clone M5/114, in-house; Rabbit anti-CC3 clone 5A1E, Cell Signaling) were incubated in 0.1% Tween 20 (Sigma-Aldrich), 0.2% BSA in PBS (PBS-T) for three days, then washed ten times with PBS-T over 5–8 h. Secondary antibodies (Donkey anti-rabbit Alexa fluor 647; Goat anti-rat Alexa fluor 488; Invitrogen), DAPI (Invitrogen; 4 µg/mL) and Phalloidin-Alexa Fluor 555 (Invitrogen; 1/25 dilution) were incubated and washed as for primary antibodies. The skin was cleared overnight in FUnGI clearing agent (Rios et al., 2019), then pressed between a glass slide and a coverslip for 3D confocal imaging with a Leica SP8 microscope equipped with an HCX PL APO ×40/1.30 NA oil objective. Images were processed in Imaris (Bitplane) by digitally clipping the dermis and recording snapshots. MHCII signal threshold for snapshots was determined by matching the intensity for LCs in non-lesion areas. The area covered by CC3, MHCII or epidermal cell junctions was measured from snapshots in ImageJ (NIH) by manual signal thresholding or region outlining relative to the total tissue or lesion/non-lesion area.

Preparation of skin for flow cytometry analysis

Mice for analysis were sacrificed, their entire torso shaved, the residual fur removed with Nair, and subcutaneous fat was removed by scraping with a scalpel blade. For separate dermis and epidermis analysis, strips of skin (1 cm × 2 cm × 2 cm) were incubated for 1 hour at 37°C in 2 U/mL of Dispase (GIBCO). Following this treatment, epidermal sheets were peeled from the dermis to separate. For dermal analysis, only a small piece (approx. 2 cm × 2 cm) was retained for further digestion. Epidermis and dermis were then cut into fine pieces and digested with 50 U/mL of collagenase for 45 min at 37°C. For whole skin analysis, approx 2 cm × 2 cm of skin was cut into fine pieces, and the tissue was then digested in 0.1 mg/mL LiberaseTM (Roche, Switzerland) and 50 µg/mL DNase I (Roche) for 2 h at 37°C under gentle agitation. Digested tissue was filtered through a 70 µm cell strainer and washed in FACS buffer (PBS + 2 mM ethylene-diamine-tetra-acetic acid (EDTA) and 0.5% Bovine Serum Albumin (BSA)). FC block (anti-CD16/CD32, 1/100; BD, NJ, USA) was added for 1 h before addition of antibody cocktail as appropriate for the particular experiment. The cells were finally washed with FACS buffer (PBS + 1% BSA) and analysed using a Fortessa X20 (BD). The data were analysed using FlowJo.

Antibodies used for flow cytometry in this project are BUV 785 Anti-mouse CD45.2 (104) (BD), Brilliant Violet 711 Anti-mouse CD45.2 (104) (Biolegend; CA, USA), BUV 395 Anti-mouse CD45.2 (104) (BD), APC Anti-mouse TCRb (H57-597) (eBioscience, CA, USA), PE Anti-mouse TCR-γδ (GL3) (BD), FITC Anti-mouse MHC II (M5) (eBioscience), Brilliant Violet 500 Anti-mouse MHCII (M5) (BD), APC-Cy7 Anti-mouse MHC II (M5) (eBioscience), PE Anti-mouse MHC II (M5) (eBioscience), Brilliant Violet 786 Anti-mouse CD11b (M1/70) (Biolegend), eFluor450 Anti-mouse CD11b (M1/70) (eBioscience), PeCy7 Anti-mouse CD11c (N418) (eBioscience), FITC Anti-mouse CD11c (N418) (WELI), Brilliant Violet 605 Anti-mouse CD64 (X54-5/7.1) (Biolegend), APC Anti-mouse XCR1 (ZET) (Biolegend), Brilliant Violet 650 XCR1 (ZET) (Biolegend), APC Anti-mouse CD326 (G8.8) (Biolegend), APC-CY7 Anti-mouse CD326 (G8.8) (Biolegend), APC Anti-mouse CD207 (4C7) (Biolegend), V450 Anti-mouse Ly6c (AL-21) (eBiosciences), BUV 737 Anti-mouse CD80 (16-10A1) (BD), Brilliant Violet 650 Anti-mouse CD86 (GL1) (BD), PE Anti-mouse CD40 (11C1) (Invitrogen), FITC Anti-mouse Ki-67 (SolA15) (eBioscience), PerCP-Cy5.5 Anti-mouse Ly-6G/Ly-6C (RB6-8C5) (eBioscience).

Preparation of full-thickness skin samples for ELISA

Whole skin samples were lysed in death induced signalling complex (DISC) lysis buffer by placing a piece of skin approx. 100 µg in 250 µl of ice-cold DISC in a 2 mL Eppendorf tube (DISC lysis buffer comprised: 20 mM Tris pH 7.5, 2 mM EDTA, 1% Triton X-100, 150 mM sodium chloride, 10% glycerol, cComplete cocktail protease inhibitor (Roche) in H₂O). The samples were then finely diced in the tube with scissors and bead beat at 30 Hertz for 3 × 1 minute using a TissueLyser (Qiagen; Venlo, Limburg, Netherlands). The samples were then lysed on ice for 30 min, spun at 13,000 rpm for 10 min, and the supernatant retained for protein analysis (ELISA). Protein lysates were quantified using a bicinchoninic acid (BCA) protein quantification kit (Thermo Fisher Scientific; MA, USA). Samples were normalised to the same concentration of total protein within an experiment to give a total protein concentration of 10 mg/mL. TNF ELISA was performed using ebioscience kits (Thermo Fisher Scientific) following the manufacturer's protocols. Data presented are calculated as pg of cytokine/mg of total protein.

Histology and immunofluorescence

Skin samples were fixed in 10% neutral buffered formalin for 24–48 h then stored in 70% ethanol before paraffin embedding and sectioning. Frozen sections were fixed briefly (2 h) in 4% PFA, transferred to 30% sucrose overnight then embedded in optimal cutting temperature (OCT) embedding medium. All samples were sectioned for routine histology staining (haematoxylin and eosin; H&E) onto Superfrost slides (Thermo Fisher Scientific). For immunohistochemistry (IHC) and immunofluorescence (IF), Superfrost plus slides (Thermo Fisher Scientific; MA, USA) were used. Formalin Fixed, Paraffin Embedded (FFPE) sections were dewaxed and rehydrated according to standard protocols. Slides were then subjected to heat-induced antigen retrieval with boiling citrate buffer for 20 min, rinsed in Tris Buffered Saline (TBS) + 0.05% Tween (TBST), then blocked and permeabilised with 1% BSA and 0.3% Triton X-100 in TBS for 15 min. OCT embedded frozen sections were dried onto slides, permeabilised with acetone for 5 min, rehydrated in TBST, and blocked with 3% normal goat serum (NGS) and 0.3% Triton X-100 in TBS for 15 min.

For cleaved caspase-3 (CC3) Ki67 and PGP9.5 stained slides, the primary antibody was diluted in blocking solution and applied to the sections, 1/300 anti-CC3 (Cell Signalling Technology; MA, USA), 1/500 anti-Ki67 (Thermo Fisher Scientific) or 1/200 anti-PGP9.5 (Abcam, UK) and incubated overnight at 4°C. The following day, slides were rinsed 3x with TBST then blocked first for endogenous peroxidases with Dako peroxidase block (Agilent Technologies; CA, USA) for 10 min, then with Avidin blocking solution for 10 min, then Biotin blocking solution for 10 min (avidin-biotin blocking kit; Vector Laboratories, MA, USA). Slides were then incubated with a goat anti-rabbit biotinylated secondary (Vector Laboratories) 1/300 for 1 h, rinsed 3 x with TBST, then labelled with VECTASTAIN Elite ABC HRP Kit (Vector Laboratories) for 30 min, rinsed 3x with TBST and developed with DAB + substrate (Agilent Technologies). Slides were then washed thoroughly under running tap water, counterstained with haematoxylin, then dehydrated by immersion in 3 changes of 100% ethanol, 4 min each, the three changes of xylene, 4 min each, and mounted using DPX mountant. Slides stained for anti-CD3 (Agilent Technologies), anti-CD45 (BD), and anti-F4/80 (WEHI) were prepared using an Autostainer Link 48 (Agilent Technologies). IF sections were incubated overnight at 4°C with anti-langerin 1/200 (Novus Biologicals), and anti-CC3 1/300, anti-GFP 1/300, or anti-CD45.1 (eBioscience) 1/300 followed by goat anti-rat (for langerin) alexa flour (AF)-594 (Thermo Fisher Scientific), anti-rabbit (for CC3 or GFP) AF-488 (Thermo Fisher Scientific), or anti-mouse (for CD45.1) AF-488 (Thermo Fisher Scientific). IF samples were coverslipped using fluoromount with DAPI (Thermo Fisher Scientific), enabling visualisation of nuclei.

Images were taken using a DP72 microscope and cellSens imaging software (Olympus), or entire slides were scanned with a Virtual Slide Microscope (Olympus), viewed using CaseCenter (3D Histech, Hungary) and image captured on a MacBook Pro 13-inch retina display (Apple, CA, USA). Minor image processing, such as adjustments to brightness and contrast, were applied to entire images, and the same adjustments were made to all comparable images. IF images were recoloured to colourblind friendly combinations using Adobe Photoshop.

IHC quantification

Multiple images totalling a minimum of three horizontal mm, encompassing dermis and epidermis, were taken from each sample for quantification. Quantitation of positively-stained cells in Ki67, CD45, CD3 and F480 stained sections was performed with Fiji software (Schindelin et al., 2012) using a scoring macro. Positively-stained cells in CC3 stained sections were manually counted. Due to the stratified nature of the skin, quantification was normalised as positively-stained cells per horizontal mm. Each data point represents a single animal, and a minimum of three animals were quantified for each group. Control and *Sharpin*^{cpdm} quantifications from multiple experiments were pooled and used in all relevant graphs.

Preparation and imaging of epidermal ear sheets

Epidermal ear sheets were prepared by collecting ears, clearing the fur with Nair, splitting them into the ventral and dorsal halves, and floating the split ears on 0.5 M ammonium thiocyanate epidermis side up for 35 min at 37°C. The epidermal sheet was then separated from the dermis, rinsed in PBS, fixed and permeabilised in ice-cold acetone for 20 min, washed in PBS, and stored in PBS + 0.05% Sodium Azide until staining.

Ear sheets were incubated at 4°C overnight with anti-langerin 1/200 (Novus Biologicals) diluted in 5% normal goat serum and 0.3% Triton X-100 in TBS. Washed 3x in TBST, then incubated in the dark in anti-rat AF594 (Thermo Fisher Scientific) for 1hr at room temperature. DAPI (1ug/mL) was added for the last 10 min of incubation to enable visualisation of nuclei. Sheets were rinsed 3 x in TBST, then transferred to 6 well plates containing 2 mL of TBST and allowed to rock for 1 h in the dark. The sheets were then laid flat on Superfrost plus slides and air-dried before cover slipping with Diamond antifade mountant (Thermo Fisher Scientific). Images were taken using a DP72 microscope and cellSens imaging software (Olympus).

QUANTIFICATION AND STATISTICAL ANALYSIS

Data were graphed and analysed using GraphPad Prism 8. Graphs show the mean ± SEM. All data points, where each data point represents an individual animal, are shown except for on the graphs showing clinical scoring over time. There n (number of animals) is stated on the graph for each experimental group. *Mann-Whitney U tests* were used to calculate significance values for the clinical scoring. One-tailed student's *t*-tests or Welch's *t*-tests, one-way ANOVA, or two-way ANOVA, as indicated in the figure legends, were conducted to calculate all other significance values. A p-value of >0.05 was considered not significant (ns), * indicates $p \leq 0.05$, ** for $p \leq 0.01$, *** for $p \leq 0.001$ and **** for $p < 0.0001$. Where no p-value is stated the value was not calculated due to small sample size or irrelevance.